GM-CSF orchestrates monocyte and granulocyte responses to *Cryptococcus gattii*

Short Title: GM-CSF and *Cryptococcus gattii* infection

Alison Ricafrente[1¶], Sreemoyee Acharya[1¶], Shuyi Chen[1], Adiza Abass[1], Aelita Arshakyan[1], Tyler J. Olson[1], Lena J. Heung[1,2*]

[1]Department of Medicine, Women's Guild Lung Institute, Cedars-Sinai Medical Center, Los Angeles, California, United States of America

[2]Department of Biomedical Sciences, Cedars-Sinai Medical Center, Los Angeles, California, United States of America

*Corresponding author

Email: lena.heung@cshs.org (LJH)

¶These authors contributed equally to this work.

Abstract

Cryptococcus gattii is an emerging fungal pathogen that is acquired through the respiratory tract and causes invasive infections in both immunocompromised and otherwise healthy people. Many of these apparently immunocompetent patients are subsequently found to have autoantibodies against the pleiotropic cytokine GM-CSF. In this study, we investigated the potential role of GM-CSF (or CSF2) in the host response to *C. gattii* using a murine model of infection. Interestingly, infected *Csf2*$^{-/-}$ mice were found to have significantly improved survival and decreased lung fungal burden compared to wild type (WT) mice. We determined that during *C. gattii* infection, GM-CSF promotes the differentiation of monocytes into alveolar and interstitial macrophages. When these macrophages are ablated in CCR2-DTR^{+} mice, there is a corresponding improvement in survival with decreased lung fungal burden, thus phenocopying *Csf2*$^{-/-}$ mice. WT bone marrow-derived macrophages challenged with *C. gattii* have poor antifungal activity, suggesting that monocyte-derived macrophages (moMacs) are rendered permissive for fungal proliferation. Therefore, GM-CSF and moMacs mediate immune responses that are harmful to the host. We further found that GM-CSF and moMacs preferentially promote the influx of eosinophils over neutrophils into the infected lung. This eosinophilia is associated with substantial inflammatory lung pathology. Ablation of neutrophils using Mrp8cre^{tg} iDTR^{+} mice significantly increased *C. gattii* burden in the lungs, indicating that GM-CSF and moMacs block the entry of these beneficial, fungal-clearing granulocytes during infection. Altogether, our results show that GM-CSF plays a key role in impeding host anti-fungal responses to *C. gattii* by coordinating monocyte-derived macrophages and granulocyte activity and crosstalk.

Author Summary

Cryptococcus gattii is an environmental fungus that can cause severe lung and brain infections after inhalation through the respiratory tract. *C. gattii* causes disease in patients with known immune deficits but also in individuals that are apparently healthy. Studies on otherwise healthy people who become infected with *C. gattii* suggest that they may have a previously unrecognized problem involving granulocyte macrophage-colony stimulating factor (GM-CSF), a cytokine, or messenger protein, that is an important part of the immune system. Here, we investigate the role of GM-CSF in the immune response to *C. gattii* using a mouse model of infection. We find that *C. gattii* increases GM-CSF in the lungs, leading to the influx of immune cells, including monocyte-derived macrophages and eosinophils, while inhibiting the entry of neutrophils. The macrophages and eosinophils allow the fungus to proliferate and cause inflammatory damage to the lungs, which is ultimately fatal. The absence of neutrophils also contributes to fungal growth, as these immune cells would otherwise be able to help kill the fungus. Our study provides new insight into how GM-CSF regulates immunity to *C. gattii* and has important implications as to the mechanisms that govern susceptibility to this infection.

Introduction

Cryptococcus gattii is an environmental, encapsulated yeast that is an important cause of invasive lung and brain infections in humans [1]. Known to be endemic in tropical and subtropical parts of the world, *C. gattii* subsequently caused an outbreak of cryptococcosis in 1999 in the temperate regions of British Columbia and the Pacific Northwest, thus broadening its global impact [2-4]. In contrast to its opportunistic relative *Cryptococcus neoformans*, *C. gattii* can also infect apparently healthy individuals. With mortality from *C. gattii* infections estimated between 10-33% [5-7], it is critically important to understand the distinct mechanisms *C. gattii* uses to cause disease in an expanding patient population. Indeed, the World Health Organization designated *C. gattii* one of its first fungal priority pathogens in 2022 given its disease potential and the large knowledge gaps regarding its pathogenicity [8].

Studies on *C. gattii* infections in otherwise healthy people discovered a close correlation with the presence of autoantibodies (AAb) against the cytokine granulocyte macrophage-colony stimulating factor (GM-CSF or CSF2) [9-12]. Anti-GM-CSF AAb are also linked to other fungal and bacterial infections, like aspergillosis and nocardiosis, and the lung disease pulmonary alveolar proteinosis (PAP) [13-15]. GM-CSF is a cytokine that plays a critical role in the development of myeloid cells and their effector functions in a broad range of disease states, from infections to autoimmune disorders [16, 17]. Although *C. gattii* infections are associated with anti-GM-CSF AAb, the role of GM-CSF in the immune response to this pathogen is not well understood.

81 Here, we used a fatal model of murine *C. gattii* infection to establish that GM-CSF
82 hinders clearance of infection and promotes immunopathology in the lungs. *Csf2*$^{-/-}$ mice
83 lacking GM-CSF have significantly improved survival rates and decreased lung fungal
84 burden compared to WT mice. We found that GM-CSF facilitates the differentiation of
85 CCR2^{+}Ly6C^{hi} monocytes into alveolar and interstitial macrophages and that ablating
86 these immune cells in CCR2-DTR^{+} mice phenocopies the improved infectious outcome
87 we observed in *Csf2*$^{-/-}$ mice. Using bone marrow-derived macrophages, we established
88 that monocyte-derived macrophages (moMacs) have a direct role in promoting *C. gattii*
89 proliferation because they are poorly activated when challenged with the fungus. We
90 also determined that GM-CSF and moMacs support the pulmonary infiltration of
91 eosinophils, that cause significant airway inflammation, while also blocking the entry of
92 neutrophils that would otherwise be beneficial for fungal clearance. Together, these
93 results indicate a critical role for GM-CSF in regulating a monocyte-granulocyte axis that
94 determines host outcomes during *C. gattii* infection.
95

96 # Results

97 ## GM-CSF mediates poor host outcomes after *C. gattii*

98 ## infection.

99 To evaluate the role of GM-CSF during *C. gattii* infection, we first established a fatal,
100 respiratory infection model by administering 10^5 *C. gattii* strain R265 intratracheally (i.t.)
101 to wild type (WT) C57BL/6J mice (S1 Fig). In these WT mice, total lung GM-CSF levels
102 increased after infection, peaking at Day 7 post-infection (p.i.) (Fig 1A). When *Csf2*$^{-/-}$
103 mice that lack GM-CSF were infected, they had prolonged survival with a median of 43
104 days as compared to 16 days for WT mice (Fig 1B). *Csf2*$^{-/-}$ mice were able to control
105 fungal proliferation in the lungs, while WT mice had an approximately 1 log increase in
106 lung fungal burden between Days 5 and 10 p.i. (Fig 1C). There were no significant
107 differences in mediastinal lymph node (MLN) or brain fungal burden (Figs 1D and 1E).
108 Grossly, the lungs of WT mice appeared significantly abnormal compared to that of
109 *Csf2*$^{-/-}$ mice, with enlarged, nodular lobes evident by Day 10 p.i. (Fig 1F). On histology,
110 WT mice had noticeably enlarged alveolar spaces at Day 10 p.i. compared to *Csf2*$^{-/-}$
111 mice (Figs 1G and 1H), and these spaces were replete with proliferating fungal cells
112 (Figs 1I and 1J). We also observed that fungal cells intercalated the collagen fibers
113 within the adventitial sheath between bronchi and arterioles in WT mice (Fig 1K), which
114 was not seen in *Csf2*$^{-/-}$ mice (Fig 1L). Collectively, these data demonstrate that GM-CSF
115 promotes fungal proliferation and invasion and distortion of lung architecture, leading to
116 accelerated mortality rates during *C. gattii* infection.
117

118 **Fig 1. GM-CSF mediates detrimental host responses to *Cryptococcus gattii*.**

119 (A) Pulmonary GM-CSF cytokine levels in WT mice infected with *C. gattii*. Days 3, 7,

120 and 10 cytokine data include *n*=8-10 total mice per timepoint from *N*=2 independent

121 experiments, except Day 5 data are from *n*=5 total mice from *N*=1 experiment. (B)

122 Kaplan-Meier survival curve of WT (white circles) and *Csf2*$^{-/-}$ (blue circles) mice, *n*=14-

123 15 mice per group from *N*=3 independent experiments. (C-E) Fungal burden was

124 measured in lung (C), mediastinal lymph node (D), and brain (E). For the lung data, Day

125 5 includes *n*=6-8 total mice per group from *N*=2 independent experiments, and Day 10

126 includes *n*=16-19 total mice per group from *N*=3 independent experiments. For lymph

127 node and brain data, Day 5 consists of *n*=3-4 total mice per group from *N*=1 experiment,

128 and Day 10 consists of *n*=8-10 total mice per group from *N*=2 independent experiments.

129 (F) Representative images of unaltered whole lungs surgically collected from WT and

130 *Csf2*$^{-/-}$ mice at Days 5 and 10 p.i. (G-L) Representative Masson's trichrome stain of

131 bronchovascular bundles in WT (G) and *Csf2*$^{-/-}$ (H) mice at Day 10 p.i., scale bar = 100

132 μM at 10X magnification. Black box is a magnified inset for the alveolar spaces of WT (I)

133 and *Csf2*$^{-/-}$ (J) mice, and red box is a magnified inset for the adventitial sheath of WT (K)

134 and *Csf2*$^{-/-}$ (L) mice, scale bar = 12 μM at 40X magnification. Airway (AW); Blood vessel

135 (BV); Collagen fibers (black arrows); Fungal cells (yellow arrowheads). Data presented

136 as mean ± SEM and analyzed using one-way ANOVA (A), Mantel-Cox test (B), or two-

137 way ANOVA (C-E). *, P <0.05. **, P <0.01. ****, P <0.0001.

138

GM-CSF facilitates monocyte differentiation into effector cells during *C. gattii* infection.

Since GM-CSF is known to regulate myeloid cells, we investigated what specific immune cells may be mediating downstream effects. On histology, we observed that cryptococcal cells in WT lungs were surrounded by large foamy macrophages (Fig 2A), while in *Csf2*$^{-/-}$ lungs there was a notable lack of macrophages in similar sites (Fig 2B). *Csf2*$^{-/-}$ mice are known to have a congenital defect in alveolar macrophage development [18, 19], which we confirmed in infected *Csf2*$^{-/-}$ versus WT mice by flow cytometry (Fig 2C). Additionally, interstitial macrophages are significantly reduced in *Csf2*$^{-/-}$ lungs by Day 10 p.i. compared to WT (Fig 2D). During inflammation or infection, alveolar and interstitial macrophages can be replenished by CCR2^{+}Ly6C^{hi} monocytes that are recruited to the lungs [20-23]. Despite an increase in CCR2^{+}Ly6C^{hi} monocytes in *Csf2*$^{-/-}$ lungs at Day 10 p.i. (Fig 2E), there was no corresponding increase in alveolar or interstitial macrophages (Figs 2C and 2D). CCR2^{+}Ly6C^{lo} monocytes, another derivative of CCR2^{+}Ly6C^{hi} monocytes [24, 25], are elevated in *Csf2*$^{-/-}$ mice at Day 10 p.i. (Fig 2F), and monocyte-derived dendritic cells (moDCs) are present in comparable numbers in both mouse strains (Fig 2G). These results suggest that the lack of GM-CSF limits the differentiation of recruited monocytes into macrophages, as studies have demonstrated in other infection models [26-28]. Monocyte chemoattractant protein-1 (MCP-1) or CCL2, a chemokine that mobilizes monocytes from the bone marrow, decreases in *Csf2*$^{-/-}$ lungs at Day 10 p.i., suggesting a backlog of monocytes in the lungs (Fig 2H) [29], and decreases in IL-1α and IL-1β in *Csf2*$^{-/-}$ lungs (Figs 2I and 2J) may be attributable to the absence of macrophages [30]. Taken together, these studies suggest

162 that GM-CSF regulation of monocyte differentiation into macrophages may play a key
163 role in the immune response during *C. gattii* infection.
164
165 **Fig 2. GM-CSF regulates the generation of monocyte-derived macrophages**
166 **during *C. gattii* infection.**
167 (A-B) Representative H&E staining of infected WT (A) and *Csf2*$^{-/-}$ (B) lung sections at
168 Day 10 p.i. showing pulmonary infiltrates, scale bar = 200μM at 4X magnification. Black
169 boxes indicate magnified insets in bottom panels, scale bar = 12μM at 60X
170 magnification. Foamy macrophages (white arrowhead). (C-G) Flow cytometry of lung
171 cells from WT (white circles) and *Csf2*$^{-/-}$ (blue circles) mice at Days 5 and 10 p.i.,
172 including alveolar macrophages (C), interstitial macrophages (D), Ly6C^{hi} monocytes (E),
173 Ly6C^{lo} monocytes (F), and monocyte-derived dendritic cells (moDCs) (G). (H-J)
174 Pulmonary levels of MCP-1/CCL2 (H), IL-1α (I), and IL-1β (J). For flow cytometric and
175 cytokine data, Day 5 includes *n*=3-5 total mice per group from *N*=1 experiment; Day 10
176 includes *n*=7-10 total mice per group from *N*=2 independent experiments. Data
177 presented as mean ± SEM and analyzed using two-way ANOVA (C-J). *, P <0.05. **, P
178 <0.01. *** P <0.001. ****, P <0.0001.
179

180 Ablation of monocytes and their derivatives improves host
181 outcomes after *C. gattii* infection.

182 To determine the role of monocytes and their derivative cells during *C. gattii* infection,
183 CCR2-DTR^{+} mice [31] treated with diphtheria toxin (DT) (Fig 3A) were used to ablate
184 CCR2^{+}Ly6C^{hi} monocytes, which also resulted in the expected loss of CCR2^{+}Ly6C^{lo}

185 monocytes, alveolar and interstitial macrophages, and moDCs compared to WT
186 littermate controls (S2A – S2E Figs). This ablation of monocytes and their derivatives
187 improved host outcomes, as CCR2-DTR$^+$ mice had a significantly increased survival
188 rate of 64% as compared to 13% in WT mice (Fig 3B). CCR2-DTR$^+$ mice also had a
189 significant reduction in fungi in the lungs at Days 3 and 7 p.i. (Fig 3C) and in the MLN at
190 Day 3 p.i. (Fig 3D) with no significant difference in brain fungal burden (Fig 3E).
191 Increases in GM-CSF and MCP-1/CCL2 in the lungs of CCR2-DTR$^+$ mice at Days 3 and
192 7 p.i. suggest a feedback loop in response to the loss of these cells (S2F and S2G
193 Figs). Similar to *Csf2*$^{-/-}$ mice, the lungs of CCR2-DTR$^+$ mice appeared grossly normal at
194 Day 7 p.i. (S2J Fig) with less alveolar enlargement (S2K and S2L Figs) and less fungal
195 invasion of the adventitial sheath (S2M and S2N Figs) compared to WT mice. Thus, the
196 absence of monocytes and their derivatives improves host outcomes after *C. gattii*
197 infection in a similar pattern as when GM-CSF is absent.
198
199 **Fig 3. Monocytes and monocyte-derived macrophages are permissive for *C. gattii***
200 **infection.**
201 (A) Monocyte ablation strategy using CCR2-DTR$^+$ and WT littermate mice, treated with
202 200 ng of diphtheria toxin by i.p. injection a day prior to infection with *C. gattii* and at
203 Days 1 and 3 p.i. Organs were harvested at Day 3 or 7 p.i. for fungal burden
204 measurements. (B) Kaplan-Meier survival curve of WT littermate (white circles) and
205 CCR2-DTR$^+$ (gray circles) mice, n=28-31 total mice per group from N=6 independent
206 experiments. (C-E) Fungal burden was measured in lung (C), MLN (D), and brain (E).
207 For lungs, Day 3 includes n=24-26 total mice per group from N=6 independent

208 experiments; Day 7 includes *n*=8-9 total mice per group from *N*=2 independent
209 experiments. For MLN and brains, Day 3 consists of *n*=18-21 total mice per group from
210 *N*=5 independent experiments; Day 7 consists of *n*=10-11 total mice per group from
211 *N*=2 independent experiments. (F-I) BMDM were challenged with 2×10^4 *C. neoformans*
212 or *C. gattii* at an MOI of 1:40 and analyzed for fungal uptake (F), fungal killing (G),
213 expression of M1 and M2 polarization markers by qRT-PCR (H), and TNF cytokine
214 secretion (I). Results are from *N*=2-3 independent experiments with *n*=6-9 total
215 replicates per group. Data presented as mean ± SEM and analyzed using Mantel-Cox
216 test (B), two-way ANOVA (C-E), and Mann-Whitney test (F-I). *, P <0.05. **, P <0.01.
217 ***, P <0.001. ****, P <0.0001.
218

219 Monocyte-derived dendritic cells do not mediate immune
220 responses to *C. gattii*

221 To evaluate if moDCs play any role in determining outcomes after *C. gattii* infection, we
222 generated CCR2-Cre$^+$ MHCII$^{fl/fl}$ mice. In this mouse model, both moDCs and
223 conventional DCs (cDCs) lack MHCII for antigen presentation compared to MHCII$^{fl/fl}$
224 littermate controls (S3A Fig), as cDCs are reported to express CCR2 [32, 33]. Despite
225 the loss of MHCII expression by these DC subsets, along with a reduction in total
226 numbers of moDCs (S3B Fig), we found no differences in survival or organ fungal
227 burden in CCR2-Cre$^+$ MHCII$^{fl/fl}$ mice versus controls after *C. gattii* infection (S3C – S3F
228 Figs). These data indicate that moDCs and cDCs do not play a critical role in the
229 immune response to *C. gattii*. Thus, observed reductions in cDCs in *Csf2*$^{-/-}$ mice [34]
230 (S4G and S4H Figs) and in moDCs and cDCs in CCR2-DTR$^+$ mice (S2E, S3I, and S3J

231 Figs) are unlikely to have contributed significantly to the phenotypes observed. Rather,
232 monocyte-derived alveolar and interstitial macrophages appear to facilitate the
233 progression of disease in our model of *C. gattii* infection.
234

235 Monocyte-derived macrophages are permissive for *C. gattii* 236 proliferation

237 To study the direct role of monocyte-derived macrophages (moMacs) in the immune
238 response to *C. gattii*, bone marrow-derived macrophages (BMDM) from WT mice were
239 challenged with *C. gattii* R265-GFP or *C. neoformans* H99-GFP [35] as a comparator.
240 We previously established that moMacs are subverted by *C. neoformans* to enable
241 fungal proliferation in the lungs [36]. When BMDM were challenged with *C. gattii*, fungal
242 uptake of *C. gattii* by BMDM was significantly reduced by an average of 41% relative to
243 the uptake seen with *C. neoformans* (Fig 3F). Although there was some killing of both
244 *C. gattii* and *C. neoformans* in the presence of BMDM, the killing of *C. gattii* by BMDM
245 was significantly impaired, with only a 48% reduction in *C. gattii* colony forming units
246 (CFUs) relative to fungus alone as compared to a 75% reduction in *C. neoformans*
247 CFUs relative to fungus alone (Fig 3G). Interestingly, *C. gattii* does not induce
248 significant polarization of BMDM since there were no changes in the expression of
249 typical markers for M1 (*Nos2* and *Tnf*) or M2 (*Arg1*, *Mrc1* and *Ym1*/*Chil3*) macrophage
250 polarization (Fig 3H). There was also no change in TNF secretion by *C. gattii*-infected
251 versus non-infected BMDM (Fig 3I). These results demonstrate that moMacs are unable
252 to effectively respond directly to *C. gattii* infection, providing an environment that allows
253 for fungal proliferation.

254

255 **GM-CSF and monocyte-derived macrophages induce**

256 **pulmonary eosinophilia**

257 When comparing our findings in *Csf2*$^{-/-}$ and CCR2-DTR^{+} mice, we observed similar
258 patterns of granulocyte infiltration into the lungs, suggesting GM-CSF and moMacs may
259 further regulate host outcomes through crosstalk with these immune cells. On lung
260 histology there was a predominance of eosinophils in perivascular infiltrates in WT
261 controls (Figs 4A and 5A), while in *Csf2*$^{-/-}$ and CCR2-DTR^{+} mice there was a clear shift
262 towards neutrophil infiltration (Figs 4B and 5B). Flow cytometry validated that total lung
263 eosinophils were significantly higher in WT controls than in *Csf2*$^{-/-}$ and CCR2-DTR^{+} mice
264 at all timepoints (Figs 4C and 5C). The relative numbers of total lung neutrophils were
265 more variable when comparing WT controls and *Csf2*$^{-/-}$ and CCR2-DTR^{+} mice over time
266 (Figs 4D and 5D). However, as infection progressed, WT controls consistently
267 demonstrated a higher eosinophil-to-neutrophil ratio in the lungs compared to either
268 *Csf2*$^{-/-}$ or CCR2-DTR^{+} mice (Figs 4E and 5E). We evaluated whole lung cytokines and
269 chemokines that might facilitate these differences in granulocyte recruitment. A key
270 finding was that the eosinophil-associated cytokine IL-5 is significantly increased in the
271 lungs of WT controls compared to *Csf2*$^{-/-}$ and CCR2-DTR^{+} mice (Figs 4F and 5F).
272 Conversely, the neutrophil-associated cytokine granulocyte-colony stimulating factor (G-
273 CSF) is suppressed in WT lungs versus *Csf2*$^{-/-}$ and CCR2-DTR^{+} mice (Figs 4G and 5G).
274 There is an increase in the cytokine subunit IL-12p40 in WT controls (Figs 4H and 5H),
275 without any change in its Th1-associated heterodimer IL-12p70 (Figs 4I and 5I) or other
276 Th1 and inflammatory cytokines (S2H-S2I, S4A and S5A Figs) as compared to *Csf2*$^{-/-}$

277 and CCR2-DTR^{+} mice. WT controls also demonstrated a skew towards higher amounts
278 of additional Th2-associated cytokines and chemokines, most prominent in comparison
279 to CCR2-DTR^{+} mice (S4B-S4C and S5B-S5C Figs), and an increase in the Th17
280 cytokine IL-17 (Figs 4J and 5J). These pro-eosinophilic conditions support clear
281 evidence of airway inflammation in WT lungs, including goblet cell hyperplasia and
282 metaplasia in the small and terminal airways and thickening of the subepithelial matrix
283 with increased collagen deposition that is not present in *Csf2*$^{-/-}$ and CCR2-DTR^{+} mice
284 (S6 Fig). These findings suggest that GM-CSF and moMacs modulate cytokines and
285 chemokines to preferentially induce pulmonary eosinophilia and inflammatory lung
286 damage after *C. gattii* infection.
287
288 **Fig 4. GM-CSF induces the pulmonary influx of eosinophils over neutrophils**
289 **during infection.**
290 (A-B) Representative H&E staining of lung sections from WT (A) and *Csf2*$^{-/-}$ (B) mice at
291 Day 10 p.i. showing perivascular cell infiltrates, scale bar = 25μM at 20X magnification.
292 Black boxes represent magnified insets in bottom panels, scale bar = 12μM at 60X
293 magnification. BV (Blood vessel). (C-E) Flow cytometry of lung cells from WT (white
294 circles) and *Csf2*$^{-/-}$ (blue circles) mice, including eosinophils (C) neutrophils (D) and the
295 calculated eosinophil-to-neutrophil (Eos:Neu) cellular ratio (E); a ratio of 1:1 is indicated
296 by the dotted line. Day 5 is n=7-9 total mice per group from N=2 independent
297 experiments; Day 10 is n=16 mice per group from N=4 independent experiments. (F-J)
298 Pulmonary levels of cytokines IL-5 (F), G-CSF (G), IL-12p40 (H), IL-12p70 (I), and IL-17
299 (J). Day 5 is n=3-10 total mice per group from N=1-2 independent experiments; Day 10

300 is *n*=8-10 total mice per group from *N*=2 independent experiments. Data presented as
301 mean ± SEM and analyzed using two-way ANOVA (C-J). *, $P < 0.05$. **, $P < 0.01$. ***, P
302 < 0.001. ****, $P < 0.0001$.
303
304 **Fig 5. Monocytes and monocyte-derived macrophages reinforce a high**
305 **eosinophil-to-neutrophil ratio in the infected lung**
306 (A-B) Representative H&E staining of lung sections from WT littermates (A) and CCR2-
307 DTR^{+} (B) mice at Day 7 p.i. showing perivascular cell infiltrates, scale bar = 25μM at
308 20X magnification. Black boxes represent magnified insets in bottom panels, scale bar =
309 12μM at 60X magnification. BV (Blood vessel). (C-E) Flow cytometry of lung cells from
310 naive WT (white triangles) and infected WT littermates (white circles) and infected *Csf2*$^{-}$
311 $^{/-}$ mice (gray circles), including eosinophils (C), neutrophils (D), and the calculated
312 Eos:Neu cellular ratio (E); a ratio of 1:1 is indicated by the dotted line. Results include
313 *n*=6 naive WT littermates from *N*=2 independent experiments and *n*=5-19 total infected
314 mice per group per timepoint from *N*=1-3 independent experiments. (F-J) Pulmonary
315 levels of cytokines IL-5 (F), G-CSF (G), IL-12p40 (H), IL-12p70 (I), and IL-17 (J).
316 Results are from *n*=8-9 total mice per group per timepoint from *N*=2 experiments. Data
317 presented as mean ± SEM and analyzed using two-way ANOVA (C-J). *, $P < 0.05$. **,
318 $P < 0.01$. ***, $P < 0.001$. ****, $P < 0.0001$.
319
320

321 ## GM-CSF and monocyte-derived macrophages suppress
322 ## neutrophil influx to promote *C. gattii* proliferation

323 To determine if the reduction in pulmonary neutrophils observed in WT control mice
324 affects progression of *C. gattii* infection, we utilized Mrp8cre^{tg} iDTR^{+} mice to deplete
325 these cells by i.p. injection of diphtheria toxin (Fig 6A) [37]. The Mrp8cre^{tg} iDTR^{+} mice
326 were infected alongside iDTR^{+} littermate controls, and then whole lungs were collected
327 for analysis. We observed an approximately 90% (1 log) decrease in lung neutrophils in
328 Mrp8cre^{tg} iDTR^{+} mice at Day 7 p.i. compared to controls (Fig 6B). This loss of
329 neutrophils in Mrp8cre^{tg} iDTR^{+} mice resulted in a significant increase in lung fungal
330 burden versus control mice (Fig 6C), suggesting neutrophils are beneficial for limiting *C.*
331 *gattii* growth in the lungs. Thus, the absence of antifungal neutrophils in combination
332 with the presence of permissive moMacs and pulmonary eosinophilia, all driven by GM-
333 CSF, provides an optimal environment for fungal proliferation and lung damage
334 resulting in host mortality.
335

336 **Fig 6. Neutrophils are beneficial to the host after *C. gattii* infection.**
337 (A) Neutrophil ablation strategy using Mrp8cre^{tg} iDTR^{+} mice and iDTR^{+} littermate control
338 mice. All mice were treated with 200 ng of diphtheria toxin by i.p. injection daily, starting
339 one day prior to i.t. infection with *C. gattii*. At Day 7 p.i., whole lungs were collected to
340 measure total neutrophils by flow cytometry (B) and fungal burden by CFU (C). Results
341 are from n=9-12 total mice per group from N=3 independent experiments. Data
342 presented as mean ± SEM and analyzed using Mann-Whitney test. *, $P < 0.05$. ****, P
343 <0.0001.

344

345 # Discussion

346 Although *C. gattii* was recognized as an emerging fungal pathogen over 25 years ago
347 [38-40], our understanding of its interactions with the host immune system that lead to
348 infection remains disproportionally limited. In this study, we establish that *C. gattii* induces
349 GM-CSF signaling in the lungs, resulting in poor infectious outcomes. Our findings
350 contrast with a recent study in which administration of recombinant murine GM-CSF led
351 to decreased amounts of *C. gattii* in the lungs [41]. However, that study used a non-fatal
352 infection model with BALB/c mice that are inherently more resistant to *C. gattii* than the
353 C57BL/6J mice used in our work [41, 42]. We instead found that physiologically elevated
354 levels of GM-CSF in the lungs of C57BL/6J mice are associated with significantly
355 increased *C. gattii* burden, immunopathology, and accelerated mortality rates. Thus, GM-
356 CSF may play different roles in acute versus chronic infection, as has also been observed
357 with *C. neoformans* [27, 43-46].

358

359 Based on our studies, GM-CSF facilitates the differentiation of recruited $CCR2^{+}Ly6C^{hi}$
360 monocytes into alveolar and interstitial macrophages after *C. gattii* infection.
361 *Cryptococcus* species are facultative intracellular pathogens [1], so these moMacs may
362 be providing a reservoir for fungal cells. Indeed, we observed that BMDM were less able
363 to control *C. gattii* as compared to *C. neoformans*; in previous work, we established that
364 moMacs are already very permissive for *C. neoformans* proliferation [36]. Interestingly,
365 *C. gattii* has reduced uptake by BMDM compared to *C. neoformans*. However, clinical
366 isolates of *C. gattii* were shown to have increased intracellular proliferation in

367 macrophages despite lower phagocytosis rates when measured alongside *C.*
368 *neoformans* [47]. BMDM also do not seem to polarize significantly and exhibit no change
369 in TNF secretion in response to *C. gattii*. Previous studies have highlighted the immune
370 silencing capacity of *C. gattii* that includes inhibition of genes associated with macrophage
371 autophagy and polarization [48]. Thus, *C. gattii* can efficiently take advantage of moMacs
372 generated under the direction of GM-CSF.
373
374 Granulocytes also appear to have a significant role downstream of GM-CSF and MoMacs
375 during infection. The worse infectious outcomes in WT mice, as compared to both *Csf2*$^{-/-}$
376 and CCR2-DTR^{+} mice, are associated with an increase in eosinophils and a decrease in
377 neutrophils in the lungs. Eosinophils have well-established roles in a wide range of
378 inflammatory pulmonary disorders like asthma and COPD [49-51]. Accordingly, the
379 pulmonary eosinophilia we see in WT mice is associated with significant airway
380 remodeling including goblet cell hyperplasia and metaplasia and collagen deposition in a
381 thickened subepithelial matrix, similar to that described in asthma [52, 53]. GM-CSF is
382 known to promote the accumulation and survival of eosinophils in allergic airway
383 inflammation [54], and macrophages can play a role in recruiting eosinophils to peripheral
384 tissues [55]. We also see increases in other cytokines in WT mice that can promote
385 eosinophils, including IL-5, IL-12p40, and IL-17. IL-5 has established roles in supporting
386 the development, accumulation, and activity of eosinophils [54, 56]. IL-12p40 can be
387 secreted by macrophages and monocytes [57], and as a free monomer or homodimer,
388 IL-12p40/IL-12p80 can act as an antagonist of IL-12 signaling [58-61]. IL-12 signaling
389 could otherwise induce apoptosis by eosinophils and promote antimicrobial neutrophil

390 activity [62, 63]. IL-17 (or IL-17A) is generally known to drive neutrophil responses [64],
391 but it can also induce pulmonary eosinophilia during allergic aspergillosis [65] and be
392 further secreted by eosinophils themselves [66]. The absence of neutrophils in the
393 infected WT lung is likely due, in part, to the observed decreased levels of G-CSF, a
394 cytokine that typically promotes neutrophil migration and activity in peripheral tissues, in
395 addition to its role in granulopoiesis [67]. This lack of neutrophil influx is significant, as we
396 demonstrate that neutrophil-depleted mice are unable to control *C. gattii* proliferation in
397 the lungs. Previous in vitro studies have also found that mouse and human neutrophils
398 have fungicidal activity against *C. gattii* [41, 68]. In sum, GM-CSF may have direct and
399 indirect roles, via moMacs and other immune cells, in the control of granulocyte influx and
400 subsequent pathology that develops during *C. gattii* infection (Fig 7).
401
402 **Fig 7. Schematic model of GM-CSF and monocyte signaling during *Cryptococcus***
403 ***gattii* infection.**
404 After *C. gattii* enters the lungs, the fungus may induce various cells, such as Type I
405 (AECI), Type II alveolar epithelial cells (AECII), endothelial cells, or fibroblasts to
406 release GM-CSF. This GM-CSF induces recruited $CCR2^{+}Ly6C^{hi}$ monocytes to
407 differentiate into alveolar and interstitial macrophages. However, these macrophages
408 remain in an unpolarized M0 state, which enables *C. gattii* to proliferate and invade host
409 tissues unchecked. GM-CSF and monocyte-derived macrophages also facilitate the
410 pulmonary influx of eosinophils while inhibiting the entry of neutrophils through the
411 regulation of cytokines including IL-5, G-CSF, IL-12p40, and IL-17. The accumulation of
412 eosinophils leads to harmful airway inflammation. The absence of antifungal neutrophils

413 allows further fungal proliferation. Altogether, the secretion of GM-CSF and the
414 generation of monocyte-derived macrophages fuel an imbalance of eosinophils and
415 neutrophils that ultimately results in host mortality. Created in BioRender. Ricafrente, A.
416 (2025) https://BioRender.com/lpowwec
417
418 We recognize that our study has only addressed some facets of how GM-CSF may
419 regulate *C. gattii* infection, and it remains to be investigated if these mechanisms are
420 recapitulated in human models. Although GM-CSF is linked to beneficial host responses
421 in other fungal diseases [27, 43-45, 69-72], there is some precedent for GM-CSF
422 increasing susceptibility to infections. In particular, pulmonary GM-CSF has been linked
423 to worse clinical outcomes for severe COVID-19 due to its role in dysregulation of
424 myeloid cells [73, 74]. This observation has led to trials on the use of anti-GM-CSF
425 monoclonal antibodies as potential treatments for COVID [75, 76]. While our work did
426 not directly study the role of anti-GM-CSF AAb, our findings challenge the prevailing
427 idea that these autoantibodies increase susceptibility to *C. gattii* [12, 77]. Thus, it
428 remains a possibility that anti-GM-CSF AAb do not play a pathogenic role in
429 cryptococcosis, which could explain why their serum levels or degree of neutralization
430 activity do not seem to have a direct correlation to the development of disease [12, 78].
431 Rather, the induction of GM-CSF by *C. gattii* may set up conditions for
432 autoimmunization, resulting in the development of anti-cytokine autoantibodies which
433 can be a physiologic process in healthy people to help maintain homeostasis [79, 80].
434 We also note that although the phenotypes of *Csf2*$^{-/-}$ and CCR2-DTR^{+} mice are very
435 similar, some features do not fully overlap and, thus, indicate the presence of

436 mechanisms that may be regulated by GM-CSF or monocytic cells independently. For
437 example, CCR2-DTR^{+} mice exhibit sustained survival during the observation period
438 while *Csf2*$^{-/-}$ mice only have delayed mortality, suggesting monocytes and their
439 derivatives have a more encompassing impact on infectious outcomes than GM-CSF
440 alone. Additionally, CCR2-DTR^{+} mice had more profound decreases in Th2-associated
441 cytokine responses in the lungs compared to *Csf2*$^{-/-}$ mice. Future work using targeted,
442 cell-specific approaches will help to further define the attributable downstream effects of
443 GM-CSF versus monocytes and to identify additional cells and signaling molecules that
444 may facilitate their roles in host immunity.
445
446 While we still have much to learn about how *C. gattii* causes disease, our study
447 provides additional insight into the key cell types and signaling pathways that are critical
448 to host susceptibility. We have established a new role for GM-CSF signaling in the
449 pathogenesis of *C. gattii* through its regulation of moMacs and crosstalk with
450 granulocytes during cryptococcosis. This work lays a foundation for further investigation
451 of GM-CSF, monocytes, and moMacs as potential immunomodulatory targets to reduce
452 mortality and other complications from *C. gattii* infection.
453
454
455
456
457

458 # Materials and Methods

459

460 ## Preparation of Cryptococcus

461 *C. gattii* strain VGIIa R265 (MYA-4093) was obtained from ATCC. *C. neoformans* strain
462 H99 #4413 was kindly provided by Joseph Heitman (Duke University). Fluorescent
463 strains R265-GFP and H99-GFP were a generous gift from Robin May (University of
464 Birmingham)[35]. All *Cryptococcus* strains were grown on Sabouraud dextrose agar
465 (SAB) plates from frozen glycerol stocks and then cultured overnight at 37°C in YPD
466 broth (1% yeast extract, 2% peptone, 2% dextrose). Fungal cells were washed three
467 times with sterile phosphate-buffered saline (PBS) and resuspended in PBS for further
468 use.

469

470 ## Mice

471 Mice were used at 6-8 weeks of age, unless otherwise noted. C57BL/6J (strain
472 #000664), B6.129X1-*H2-Ab1*$^{b\text{-}tm1Koni}$/J (strain #013181, referred to as MHCII$^{fl/fl}$), and
473 *Csf2*$^{-/-}$ (strain #026812) mice were purchased from Jackson Laboratory. MRP8-Cre-
474 ires/GFP^{+} ROSA26iDTR^{+} mice (referred to as Mrp8cre^{Tg} iDTR^{+} mice) were generated
475 using Jackson strains #021614 and #007900 and were generously provided by Keith
476 Chan (Houston Methodist). The CCR2-DTR^{+} and CCR2-Cre^{+} mice were generated as
477 previously described [31, 36]. All mouse strains were bred and housed in the Cedars-
478 Sinai Medical Center vivarium under specific pathogen-free conditions. Experiments
479 using CCR2-DTR^{+}, CCR2-Cre^{+} MHCII$^{fl/fl}$, and Mrp8cre^{Tg} iDTR^{+} mice included littermate

480 control mice that were weaned from the same litters and co-housed. The genotypes of
481 CCR2-DTR^{+} mice were validated by the presence of CD45^{+}CD11b^{+}CFP^{+} cells in tail
482 vein blood samples using flow cytometry as previously described [31]. The genotypes of
483 Mrp8cre^{Tg} mice were validated by the presence of CD11b^{+}Ly6G^{+}GFP^{+} cells in tail vein
484 blood samples using flow cytometry. The genotypes of CCR2-Cre^{+}, MHCII$^{fl/fl}$, and
485 ROSA26iDTR^{+} (referred to as iDTR^{+}) mice were validated by PCR of ear DNA as
486 previously described [36] or as per Jackson Laboratory protocol.
487

488 Ethics statement

489 All animal procedures were performed with approval by the Institutional Animal Care
490 and Use Committee at Cedars-Sinai Medical Center under protocol 8429 and were
491 compliant with all applicable provisions established by the Animal Welfare Act and the
492 Public Health Services Policy on the Humane Care and Use of Laboratory Animals.
493

494 Murine infection with *Cryptococcus gattii*

495 Overnight YPD broth cultures of *C. gattii* R265 were washed three times with sterile
496 PBS and resuspended at a concentration of 10^5 cells per 50 μL volume. Mice were
497 anesthetized with inhaled isoflurane and 50 μL of the fungal cell suspension was
498 administered intratracheally (i.t.) using a blunt ended 20-gauge dispensing tip, as
499 previously described [81].
500

501 ## Immune cell ablation

502 To ablate monocytes and neutrophils, respectively, CCR2-DTR^{+} and Mrp8cre^{Tg} iDTR^{+}
503 mice with their control littermates were injected intraperitoneally (i.p.) with 200 ng (10
504 ng/g body weight) of diphtheria toxin (List Biological Laboratories) with the frequency
505 indicated in Fig 3A and Fig 6A.
506

507 ## Fungal burden in organs

508 After infection, whole organs including lungs, mediastinal lymph nodes (MLN), and
509 brains were collected from euthanized mice into sterile PBS. Lungs and brain were
510 homogenized in gentleMACS™ C tubes using a gentleMACS™ Octo Dissociator
511 (Miltenyi Biotec). Specifically, lung samples were homogenized in 5 mL PBS + 0.5%
512 Bovine Serum Albumin (BSA) (Fisher Scientific) + 2.31 mg/mL Collagenase Type 4
513 (Worthington Biochemical Corporation) + 100 mg/mL DNAse I grade II (Roche) using
514 the “Mouse Spleen 1” program, incubated at 37°C for 45 min, and further homogenized
515 using the “Mouse Lung 2” program. Brain samples were homogenized in 1 mL PBS
516 using the “Mouse Lung 2” program. MLN were mechanically dissociated using ground
517 glass slides in 1 mL PBS. Tissue homogenates were serially diluted in PBS and
518 cultured on SAB plates at 37°C. After 3 days, fungal colonies were counted and total
519 colony forming units (CFU) per organ were calculated.
520

521 ## Cytokine and chemokine measurement

522 To analyze cytokine and chemokine levels, whole mouse lungs were collected into 2 mL
523 PBS containing 1X Halt™ Protease Inhibitor Cocktail (Thermo Fisher Scientific)
524 followed by mechanical tissue dissociation using gentleMACS™ C tubes and the "RNA
525 1" program on a gentleMACS™ Octo Dissociator (Miltenyi Biotec). Tissue homogenates
526 were centrifuged at 1500 rpm to remove cell debris, and the supernatant was collected.
527 Supernatants were processed using the Bio-Plex Pro Mouse Cytokine 23-Plex Assay
528 (Bio-Rad) and analyzed on a Bio-Plex 200 System (Bio-Rad).
529

530 ## Flow cytometry

531 For flow cytometry analysis of whole lungs, single cell suspensions were generated
532 using mechanical tissue dissociation and digestion as described in the "Fungal burden
533 in organs" section of the Materials and Methods. Isolated cells were treated with 1X
534 RBC lysis buffer for 5 min and then washed with 0.5% BSA in PBS before being passed
535 through a 100 μM cell strainer. Total cells were counted using a hemocytometer and
536 then stained with fluorescent antibodies (S1 Table). Flow cytometry data was collected
537 on a LSRFortessa (BD Biosciences) and analyzed with FlowJo software v10.10. Gating
538 strategies are shown in S7-S9 Figs.
539

540 ## Histopathology

541 The lungs of euthanized mice were instilled with 4% paraformaldehyde (PFA) in PBS *in*
542 *situ* via a catheter inserted through an incision in the trachea. The lungs were then

543 harvested and fixed by immersion in 4% PFA overnight and stored in 70% ethanol until
544 processing. Lungs were embedded in paraffin using an ASP300S tissue processor
545 (Leica), and 5 μm sections were generated using a Microm HM 325 microtome (Thermo
546 Fisher Scientific). Lung sections were stained with StatLab™ Masson's Trichrome stain
547 kit (Fisher Scientific) or Harris Hematoxylin Solution, Modified (Millipore Sigma) and
548 Eosin Y solution, Alcoholic (Millipore Sigma) (H&E). Images were captured using a
549 Nikon Ti2 microscope. Figure images shown of WT and *Csf2*$^{-/-}$ stained lung sections at
550 Day 10 p.i. represent *n*=4-5 mice per group from *N*=1 experiment. Figure images shown
551 of WT littermate and CCR2-DTR^{+} stained lung sections at Day 7 p.i. represent *n*=5 mice
552 per group from *N*=1 experiment.
553

554 Bone-marrow derived macrophage studies

555 Bone-marrow derived macrophages (BMDM) were generated from C57BL/6J mouse
556 bone marrow using L929 cell-conditioned medium, as previously described [82]. Freshly
557 cultured R265-GFP and H99-GFP cells were opsonized for 1 hr at room temperature
558 with murine anti-glucuronoxylomannan monoclonal antibody 18B7, kindly provided by
559 Arturo Casadevall (Johns Hopkins), at a concentration 10 ug/mL in DMEM media.
560 Opsonized fungal cells were used to challenge BMDM at a multiplicity of infection (MOI)
561 of 1:40 for 24 hours at 37°C 5% CO_2. Killing of fungal cells by BMDM was measured by
562 plating CFU from BMDM lysed in water. Uptake of the fluorescent fungal cells by BMDM
563 was measured by flow cytometry analysis on an LSRFortessa (BD Biosciences). Mouse
564 TNF cytokine secretion was measured by ELISA (Invitrogen) on cell culture supernatant
565 using a Varioskan Lux Multimode Microplate Reader (Thermo Fisher Scientific). For

566 quantitative RT-PCR, total RNA was extracted from BMDM using TRIzol LS (Thermo
567 Fisher Scientific), and cDNA was generated using a High Capacity RNA to cDNA Kit
568 (Applied Biosystems). The cDNA was inspected and normalized using a Nanodrop
569 Spectrophotometer (Thermo Fisher Scientific), and qRT-PCR was performed on a ViiA
570 7 Real-Time PCR System (Applied Biosystems) using TaqMan Fast Advanced Master
571 Mix and TaqMan Gene Expression Assays (Thermo Fisher Scientific), including Arg1
572 (Mm00475988_m1), Mrc1 (Mm01329362_m1), Retnla/Fizz1 (Mm00445109_m1), Hprt
573 (Mm03024075_m1), Nos2 (Mm00440502_m1), Tnf (Mm00443258_m1), and Chil3/Ym1
574 (Mm00657889_mH). Relative expression of transcripts was normalized using Hprt as a
575 housekeeping gene.
576

577 ## Statistical analysis

578 All results were expressed as mean ± SEM. A Mann-Whitney U test was used for
579 statistical analysis of two group comparisons, one-way ANOVA was used for 3 or more
580 infected mouse groups, and two-way ANOVA was used for 3 or more naive and infected
581 mouse groups, unless otherwise noted. Survival data was analyzed by Mantel-Cox test.
582 All statistical analyses were performed with GraphPad Prism software, v10.2.0. A P
583 value < 0.05 was considered significant and indicated with an asterisk.
584

585 ## Acknowledgments

586 We thank Fayyaz Sutterwala, Suzanne Cassel, and Apurwa Trivedi for helpful
587 comments and all our colleagues in the Women's Guild Lung Institute and Research
588 Division of Immunology, Keith Chan, and Fotis Nikolos for generously sharing materials,

589 equipment, and their expertise. We acknowledge assistance from the Cedars-Sinai
590 Flow Cytometry Shared Resource and Biobank and Research Pathology Resource.
591

References

1. Heitman J, Kozel, T. R., Kwon-Chung, K. J., Perfect, J. R. and Casadevall A. *Cryptococcus*: from human pathogen to model yeast. 1 ed: ASM Press; 2010 November 12, 2010. 1-646 p.
2. Stephen C, Lester S, Black W, Fyfe M, Raverty S. Multispecies outbreak of cryptococcosis on southern Vancouver Island, British Columbia. Can Vet J. 2002;43(10):792-4. pmid:12395765.
3. Hoang LM, Maguire JA, Doyle P, Fyfe M, Roscoe DL. *Cryptococcus neoformans* infections at Vancouver Hospital and Health Sciences Centre (1997–2002): epidemiology, microbiology and histopathology. J Med Microbiol. 2004;53(9):935-40. pmid:15314203.
4. Casalini G, Giacomelli A, Antinori S. The WHO fungal priority pathogens list: a crucial reappraisal to review the prioritisation. Lancet Microbe. 2024;5(7):717-24.
5. Galanis E, Macdougall L, Kidd S, Morshed M. Epidemiology of *Cryptococcus gattii*, British Columbia, Canada, 1999-2007. Emerg Infect Dis. 2010;16(2):251-7. pmid:20113555.
6. Harris JR, Lockhart SR, Debess E, Marsden-Haug N, Goldoft M, Wohrle R, et al. *Cryptococcus gattii* in the United States: clinical aspects of infection with an emerging pathogen. Clin Infect Dis. 2011;53(12):1188-95. Epub 20111019. pmid:22016503.
7. Harris JR, Lockhart SR, Sondermeyer G, Vugia DJ, Crist MB, D'Angelo MT, et al. *Cryptococcus gattii* infections in multiple states outside the US Pacific Northwest. Emerg Infect Dis. 2013;19(10):1620-6. pmid:24050410.
8. WHO. WHO fungal priority pathogens list to guide research, development and public health action.: World Health Organization; 2022. Available from: https://www.who.int/publications/i/item/9789240060241
9. Rosen LB, Freeman AF, Yang LM, Jutivorakool K, Olivier KN, Angkasekwinai N, et al. Anti-GM-CSF autoantibodies in patients with cryptococcal meningitis. J Immunol. 2013;190(8):3959-66. pmid:23509356.
10. Jiang YK, Zhou LH, Cheng JH, Zhu JH, Luo Y, Li L, et al. Anti-GM-CSF autoantibodies predict outcome of cryptococcal meningitis in patients not infected with HIV: A cohort study. Clin Microbiol Infect. 2024;30(5):660-5. Epub 20240129. pmid:38295989.
11. Kuo PH, Wu UI, Pan YH, Wang JT, Wang YC, Sun HY, et al. Neutralizing anti-granulocyte-macrophage colony-Stimulating factor autoantibodies in patients with central nervous system and localized cryptococcosis: longitudinal follow-up and literature Review. Clin Infect Dis. 2022;75(2):278-87. pmid:34718451.
12. Wang S-Y, Lo Y-F, Shih H-P, Ho M-W, Yeh C-F, Peng J-J, et al. *Cryptococcus gattii* infection as the major clinical manifestation in patients with autoantibodies against granulocyte–macrophage colony-stimulating factor J Clin Immunol. 2022;42(8):1730-41. pmid:35947322.

633 13. Ataya A, Knight V, Carey BC, Lee E, Tarling EJ, Wang T. The role of GM-CSF
634 autoantibodies in infection and autoimmune pulmonary alveolar proteinosis: a concise
635 review. Front Immunol. 2021;12:752856. Epub 2021/12/10. pmid:34880857.
636 14. Punatar AD, Kusne S, Blair JE, Seville MT, Vikram HR. Opportunistic infections
637 in patients with pulmonary alveolar proteinosis. J Infect. 2012;65(2):173-9. Epub
638 2012/04/10. pmid:22484272.
639 15. Rosen LB, Rocha Pereira N, Figueiredo C, Fiske LC, Ressner RA, Hong JC, et
640 al. Nocardia-induced granulocyte macrophage colony-stimulating factor is neutralized
641 by autoantibodies in disseminated/extrapulmonary nocardiosis. Clin Infect Dis.
642 2015;60(7):1017-25. Epub 20141203. pmid:25472947.
643 16. Becher B, Tugues S, Greter M. GM-CSF: From growth factor to central mediator
644 of tissue inflammation Immunity. 2016;45(5):963-73. Epub 2016/11/17. pmid:27851925.
645 17. Chen Y, Li F, Hua M, Liang M, Song C. Role of GM-CSF in lung balance and
646 disease. Front Immunol. 2023;14:1158859. Epub 2023/04/21. pmid:37081870.
647 18. Stanley E, Lieschke GJ, Grail D, Metcalf D, Hodgson G, Gall JA, et al.
648 Granulocyte/macrophage colony-stimulating factor-deficient mice show no major
649 perturbation of hematopoiesis but develop a characteristic pulmonary pathology. Proc
650 Natl Acad Sci U S A. 1994;91(12):5592-6. Epub 1994/06/07. pmid:8202532.
651 19. Guilliams M, De Kleer I, Henri S, Post S, Vanhoutte L, De Prijck S, et al. Alveolar
652 macrophages develop from fetal monocytes that differentiate into long-lived cells in the
653 first week of life via GM-CSF. J Exp Med. 2013;210(10):1977-92. Epub 2013/09/18.
654 pmid:24043763.
655 20. Misharin AV, Morales-Nebreda L, Reyfman PA, Cuda CM, Walter JM, McQuattie-
656 Pimentel AC, et al. Monocyte-derived alveolar macrophages drive lung fibrosis and
657 persist in the lung over the life span. J Exp Med. 2017;214(8):2387-404. Epub
658 2017/07/12. pmid:28694385.
659 21. Machiels B, Dourcy M, Xiao X, Javaux J, Mesnil C, Sabatel C, et al. A
660 gammaherpesvirus provides protection against allergic asthma by inducing the
661 replacement of resident alveolar macrophages with regulatory monocytes. Nat Immunol.
662 2017;18(12):1310-20. Epub 2017/10/17. pmid:29035391.
663 22. Aegerter H, Kulikauskaite J, Crotta S, Patel H, Kelly G, Hessel EM, et al.
664 Influenza-induced monocyte-derived alveolar macrophages confer prolonged
665 antibacterial protection. Nat Immunol. 2020;21(2):145-57. Epub 2020/01/15.
666 pmid:31932810.
667 23. Evren E, Ringqvist E, Tripathi KP, Sleiers N, Rives IC, Alisjahbana A, et al.
668 Distinct developmental pathways from blood monocytes generate human lung
669 macrophage diversity. Immunity. 2021;54(2):259-75.e7.
670 24. Dal-Secco D, Wang J, Zeng Z, Kolaczkowska E, Wong CH, Petri B, et al. A
671 dynamic spectrum of monocytes arising from the in situ reprogramming of CCR2+
672 monocytes at a site of sterile injury. J Exp Med. 2015;212(4):447-56. Epub 2015/03/25.
673 pmid:25800956.
674 25. Mildner A, Schönheit J, Giladi A, David E, Lara-Astiaso D, Lorenzo-Vivas E, et al.
675 Genomic Characterization of Murine Monocytes Reveals C/EBPβ Transcription
676 Factor Dependence of Ly6C[−] Cells. Immunity. 2017;46(5):849-
677 62.e7.

678 26. Shibata Y, Berclaz PY, Chroneos ZC, Yoshida M, Whitsett JA, Trapnell BC. GM-
679 CSF regulates alveolar macrophage differentiation and innate immunity in the lung
680 through PU.1. Immunity. 2001;15(4):557-67. Epub 2001/10/24. pmid:11672538.
681 27. Chen G-H, Teitz-Tennenbaum S, Neal LM, Murdock BJ, Malachowski AN, Dils
682 AJ, et al. Local GM-CSF–dependent differentiation and activation of pulmonary dendritic
683 cells and macrophages protect against progressive cryptococcal lung infection in mice J
684 Immunol. 2016;196(4):1810-21. pmid:26755822.
685 28. Osterholzer JJ, Chen GH, Olszewski MA, Curtis JL, Huffnagle GB, Toews GB.
686 Accumulation of $CD11b^{+}$ lung dendritic cells in response to fungal infection results from
687 the CCR2-mediated recruitment and differentiation of $Ly\text{-}6C^{high}$ monocytes. J Immunol.
688 2009;183(12):8044-53. pmid:19933856.
689 29. Gelman AE, Okazaki M, Sugimoto S, Li W, Kornfeld CG, Lai J, et al. CCR2
690 regulates monocyte recruitment as well as CD4 T1 allorecognition after lung
691 transplantation. Am J Transplant. 2010;10(5):1189-99. pmid:20420631.
692 30. Liu X, Boyer MA, Holmgren AM, Shin S. Legionella-infected macrophages
693 engage the alveolar epithelium to metabolically reprogram myeloid cells and promote
694 antibacterial inflammation. Cell Host Microbe. 2020;28(5):683-98.e6.
695 31. Hohl TM, Rivera A, Lipuma L, Gallegos A, Shi C, Mack M, et al. Inflammatory
696 monocytes facilitate adaptive CD4 T cell responses during respiratory fungal infection.
697 Cell Host Microbe. 2009;6(5):470-81. pmid:19917501.
698 32. Bosteels C, Fierens K, De Prijck S, Van Moorleghem J, Vanheerswynghels M,
699 De Wolf C, et al. CCR2- and Flt3-dependent inflammatory conventional type 2 dendritic
700 cells are necessary for the induction of adaptive immunity by the human vaccine
701 adjuvant system AS01. Front Immunol. 2020;11:606805. Epub 20210114.
702 pmid:33519816.
703 33. Lewis Kanako L, Caton Michele L, Bogunovic M, Greter M, Grajkowska Lucja T,
704 Ng D, et al. Notch2 receptor signaling controls functional differentiation of dendritic cells
705 in the spleen and intestine. Immunity. 2011;35(5):780-91.
706 34. Greter M, Helft J, Chow A, Hashimoto D, Mortha A, Agudo-Cantero J, et al. GM-
707 CSF controls nonlymphoid Tissue dendritic cell homeostasis but Is dispensable for the
708 differentiation of inflammatory dendritic cells. Immunity. 2012;36(6):1031-46.
709 35. Voelz K, Johnston SA, Rutherford JC, May RC. Automated analysis of
710 cryptococcal macrophage parasitism using GFP-tagged cryptococci. PLoS One.
711 2010;5(12):e15968. pmid:21209844.
712 36. Heung LJ, Hohl TM. Inflammatory monocytes are detrimental to the host immune
713 response during acute infection with *Cryptococcus neoformans*. PLoS Patho.
714 2019;15(3):e1007627. Epub 2019/03/22. pmid:30897162.
715 37. Ballesteros I, Rubio-Ponce A, Genua M, Lusito E, Kwok I, Fernández-Calvo G, et
716 al. Co-option of neutrophil fates by tissue environments. Cell. 2020;183(5):1282-97.e18.
717 38. MacDougall L, Kidd SE, Galanis E, Mak S, Leslie MJ, Cieslak PR, et al. Spread
718 of *Cryptococcus gattii* in British Columbia, Canada, and detection in the Pacific
719 Northwest, USA. Emerg Infect Dis. 2007;13(1):42-50. pmid:17370514.
720 39. MacDougall L, Fyfe M. Emergence of *Cryptococcus gattii* in a Novel Environment
721 Provides Clues to Its Incubation Period. Journal of Clinical Microbiology.
722 2006;44(5):1851-2.

723 40. Kidd SE, Hagen F, Tscharke RL, Huynh M, Bartlett KH, Fyfe M, et al. A rare
724 genotype of *Cryptococcus gattii* caused the cryptococcosis outbreak on Vancouver
725 Island (British Columbia, Canada). Proceedings of the National Academy of Sciences.
726 2004;101(49):17258-63.
727 41. Hansakon A, Khampoongern R, Schiller L, Jeerawattanawart S, Angkasekwinai
728 P. Effect of intranasal administration of granulocyte-macrophage colony-stimulating
729 factor on pulmonary *Cryptococcus gattii* infection. Int Immunopharmacol.
730 2024;142:113259. pmid:39332096.
731 42. Oliveira-Brito PKM, de Campos GY, Guimarães JG, Serafim da Costa L, Silva de
732 Moura E, Lazo-Chica JE, et al. Adjuvant curdlan contributes to immunization against
733 *Cryptococcus gattii* infection in a mouse strain-specific manner. Vaccines.
734 2022;10(4):620. pmid:10.3390/vaccines10040620.
735 43. Chen GH, Curtis JL, Mody CH, Christensen PJ, Armstrong LR, Toews GB. Effect
736 of granulocyte-macrophage colony-stimulating factor on rat alveolar macrophage
737 anticryptococcal activity *in vitro*. J Immunol. 1994;152(2):724-34.
738 44. Chen G-H, Olszewski MA, McDonald RA, Wells JC, Paine R, Huffnagle GB, et al.
739 Role of granulocyte macrophage colony-stimulating factor in host defense against
740 pulmonary *Cryptococcus neoformans* infection during murine allergic bronchopulmonary
741 mycosis Am J Pathol. 2007;170(3):1028-40. pmid:17322386.
742 45. Chiller T, Farrokhshad K, Brummer E, Stevens DA. Effect of granulocyte colony-
743 stimulating factor and granulocyte-macrophage colony-stimulating factor on
744 polymorphonuclear neutrophils, monocytes or monocyte-derived macrophages
745 combined with voriconazole against *Cryptococcus neoformans*. Med Mycol J.
746 2002;40(1):21-6. pmid:11860010.
747 46. Strickland AB, Chen Y, Sun D, Shi M. Alternatively activated lung alveolar and
748 interstitial macrophages promote fungal growth. iScience. 2023;26(5):106717.
749 47. Hansakon A, Mutthakalin P, Ngamskulrungroj P, Chayakulkeeree M,
750 Angkasekwinai P. *Cryptococcus neoformans* and *Cryptococcus gattii* clinical isolates
751 from Thailand display diverse phenotypic interactions with macrophages. Virulence.
752 2019;10(1):26-36. Epub 2018/12/07. pmid:30520685.
753 48. Piffer AC, Santos FMD, Thomé MP, Diehl C, Garcia AWA, Kinskovski UP, et al.
754 Transcriptomic analysis reveals that mTOR pathway can be modulated in macrophage
755 cells by the presence of cryptococcal cells. Genet Mol Biol. 2021;44(3):e20200390.
756 Epub 2021/08/06. pmid:34352067.
757 49. Jackson DJ, Akuthota P, Roufosse F. Eosinophils and eosinophilic immune
758 dysfunction in health and disease. Eur Respir Rev. 2022;31(163). Epub 2022/01/28.
759 pmid:35082127.
760 50. Brightling CE, Monteiro W, Ward R, Parker D, Morgan MDL, Wardlaw AJ, et al.
761 Sputum eosinophilia and short-term response to prednisolone in chronic obstructive
762 pulmonary disease: a randomised controlled trial. Lancet. 2000;356(9240):1480-5.
763 51. Brightling CE, Symon FA, Birring SS, Bradding P, Wardlaw AJ, Pavord ID.
764 Comparison of airway immunopathology of eosinophilic bronchitis and asthma. Thorax.
765 2003;58(6):528-32.
766 52. Varricchi G, Brightling CE, Grainge C, Lambrecht BN, Chanez P. Airway
767 remodelling in asthma and the epithelium: on the edge of a new era. Eur Respir J.
768 2024;63(4). Epub 2024/04/13. pmid:38609094.

769 53. Zhou Y, Duan Q, Yang D. In vitro human cell-based models to study airway
770 remodeling in asthma. Biomed Pharmacother. 2023;159:114218. Epub 2023/01/14.
771 pmid:36638596.
772 54. Nobs SP, Kayhan M, Kopf M. GM-CSF intrinsically controls eosinophil
773 accumulation in the setting of allergic airway inflammation. J Allergy Clin Immunol.
774 2019;143(4):1513-24.e2. pmid:30244025.
775 55. Voehringer D, van Rooijen N, Locksley RM. Eosinophils develop in distinct
776 stages and are recruited to peripheral sites by alternatively activated macrophages. J
777 Leukoc Biol. 2007;81(6):1434-44. Epub 2007/03/07. pmid:17339609.
778 56. Dougan M, Dranoff G, Dougan SK. GM-CSF, IL-3, and IL-5 Family of Cytokines:
779 Regulators of Inflammation. Immunity. 2019;50(4):796-811. Epub 2019/04/18.
780 pmid:30995500.
781 57. Oliveira MA, Lima GM, Shio MT, Leenen PJ, Abrahamsohn IA. Immature
782 macrophages derived from mouse bone marrow produce large amounts of IL-12p40
783 after LPS stimulation. J Leukoc Biol. 2003;74(5):857-67. pmid:14595006.
784 58. Ling P, Gately MK, Gubler U, Stern AS, Lin P, Hollfelder K, et al. Human IL-12
785 p40 homodimer binds to the IL-12 receptor but does not mediate biologic activity. J
786 Immunol. 1995;154(1):116-27. pmid:7527811.
787 59. Mattner F, Fischer S, Guckes S, Jin S, Kaulen H, Schmitt E, et al. The
788 interleukin-12 subunit p40 specifically inhibits effects of the interleukin-12 heterodimer.
789 Eur J Immunol. 1993;23(9):2202-8. Epub 1993/09/01. pmid:8103745.
790 60. Gillessen S, Carvajal D, Ling P, Podlaski FJ, Stremlo DL, Familletti PC, et al.
791 Mouse interleukin-12 (IL-12) p40 homodimer: a potent IL-12 antagonist. Eur J Immunol.
792 1995;25(1):200-6. Epub 1995/01/01. pmid:7843232.
793 61. Heinzel FP, Hujer AM, Ahmed FN, Rerko RM. In vivo production and function of
794 IL-12 p40 homodimers. J Immunol. 1997;158(9):4381-8. Epub 1997/05/01.
795 pmid:9127002.
796 62. Nutku E, Zhuang Q, Soussi-Gounni A, Aris F, Mazer BD, Hamid Q. Functional
797 expression of IL-12 receptor by human eosinophils: IL-12 promotes eosinophil
798 apoptosis. J Immunol. 2001;167(2):1039-46. pmid:11441113.
799 63. Moreno SE, Alves-Filho JC, Alfaya TM, da Silva JS, Ferreira SH, Liew FY. IL-12,
800 but not IL-18, is critical to neutrophil activation and resistance to polymicrobial sepsis
801 induced by cecal ligation and puncture. J Immunol. 2006;177(5):3218-24.
802 pmid:16920961.
803 64. McGeachy MJ, Cua DJ, Gaffen SL. The IL-17 Family of Cytokines in Health and
804 Disease. Immunity. 2019;50(4):892-906. Epub 2019/04/18. pmid:30995505.
805 65. Murdock BJ, Falkowski NR, Shreiner AB, Sadighi Akha AA, McDonald RA, White
806 ES, et al. Interleukin-17 drives pulmonary eosinophilia following repeated exposure to
807 Aspergillus fumigatus conidia. Infect Immun. 2012;80(4):1424-36. Epub 20120117.
808 pmid:22252873.
809 66. Malacco NLSdO, Rachid MA, Gurgel ILdS, Moura TR, Sucupira PHF, Sousa
810 LPd, et al. Eosinophil-associated innate IL-17 response promotes aspergillus fumigatus
811 lung pathology. Front Cell Infect Microbiol. 2019;Volume 8 - 2018.
812 67. Martin KR, Wong HL, Witko-Sarsat V, Wicks IP. G-CSF - A double edge sword in
813 neutrophil mediated immunity. Semin Immunol. 2021;54:101516. Epub 2021/11/04.
814 pmid:34728120.

815 68. Ueno K, Yanagihara N, Otani Y, Shimizu K, Kinjo Y, Miyazaki Y. Neutrophil-
816 mediated antifungal activity against highly virulent *Cryptococcus gattii* strain R265. Med
817 Mycol. 2019;57(8):1046-54. Epub 2019/01/23. pmid:30668754.
818 69. Mills KAM, Westermann F, Espinosa V, Rosiek E, Desai JV, Aufiero MA, et al.
819 GM-CSF-mediated epithelial-immune cell cross-talk orchestrates pulmonary immunity to
820 *Aspergillus fumigatus*. Sci Immunol. 2025;10(105):eadr0547.
821 70. Kasahara S, Jhingran A, Dhingra S, Salem A, Cramer RA, Hohl TM. Role of
822 granulocyte-macrophage colony-stimulating factor signaling in regulating neutrophil
823 antifungal activity and the oxidative burst during respiratory fungal challenge. J Infect
824 Dis. 2016;213(8):1289-98.
825 71. Deepe GS, Jr., Gibbons R, Woodward E. Neutralization of endogenous
826 granulocyte-macrophage colony-stimulating factor subverts the protective immune
827 response to *Histoplasma capsulatum*. J Immunol. 1999;163(9):4985-93.
828 72. Hernández-Santos N, Wiesner DL, Fites JS, McDermott AJ, Warner T, Wüthrich
829 M, et al. Lung epithelial cells coordinate innate lymphocytes and immunity against
830 pulmonary fungal infection. Cell Host Microbe. 2018;23(4):511-22.e5.
831 73. Huang C, Wang Y, Li X, Ren L, Zhao J, Hu Y, et al. Clinical features of patients
832 infected with 2019 novel coronavirus in Wuhan, China. Lancet. 2020;395(10223):497-
833 506. pmid:31986264.
834 74. Thwaites RS, Sanchez Sevilla Uruchurtu A, Siggins MK, Liew F, Russell CD,
835 Moore SC, et al. Inflammatory profiles across the spectrum of disease reveal a distinct
836 role for GM-CSF in severe COVID-19. Sci Immunol. 2021;6(57):eabg9873.
837 75. De Luca G, Cavalli G, Campochiaro C, Della-Torre E, Angelillo P, Tomelleri A, et
838 al. GM-CSF blockade with mavrilimumab in severe COVID-19 pneumonia and systemic
839 hyperinflammation: a single-centre, prospective cohort study. Lancet Rheumatol.
840 2020;2(8):e465-e73.
841 76. Temesgen Z, Burger CD, Baker J, Polk C, Libertin CR, Kelley CF, et al.
842 Lenzilumab in hospitalised patients with COVID-19 pneumonia (LIVE-AIR): a phase 3,
843 randomised, placebo-controlled trial. Lancet Respir Med. 2022;10(3):237-46.
844 77. Arango-Franco CA, Rojas J, Firacative C, Migaud M, Agudelo CI, Franco JL, et
845 al. Autoantibodies neutralizing GM-CSF in HIV-negative Colombian patients infected
846 with *Cryptococcus gattii* and *C. neoformans*. J Clin Immunol. 2024;44(7):163.
847 78. Salvator H, Cheng A, Rosen LB, Williamson PR, Bennett JE, Kashyap A, et al.
848 Neutralizing GM-CSF autoantibodies in pulmonary alveolar proteinosis, cryptococcal
849 meningitis and severe nocardiosis. Respir Res. 2022;23(1):280. Epub 2022/10/12.
850 pmid:36221098.
851 79. Vincent T, Plawecki M, Goulabchand R, Guilpain P, Eliaou JF. Emerging clinical
852 phenotypes associated with anti-cytokine autoantibodies. Autoimmun Rev.
853 2015;14(6):528-35.
854 80. Cappellano G, Orilieri E, Woldetsadik AD, Boggio E, Soluri MF, Comi C, et al.
855 Anti-cytokine autoantibodies in autoimmune diseases. Am J Clin Exp Immunol.
856 2012;1(2):136-46. Epub 20121115. pmid:23885320.
857 81. Jhingran A, Kasahara S, Hohl TM. Flow cytometry of lung and bronchoalveolar
858 lavage fluid cells from mice challenged with Fluorescent Aspergillus Reporter (FLARE)
859 Conidia. Bio Protoc. 2016;6(18). pmid:28691040.

860 82. Heung LJ, Hohl TM. DAP12 inhibits pulmonary immune responses to
861 *Cryptococcus neoformans*. Infect Immun. 2016;84(6):1879-86. pmid:27068093.
862

863 # Supporting Information

864

865 **S1 Fig. Kaplan-Meier survival curve of wild type mice infected with different**

866 **inocula of *Cryptococcus gattii* R265 intratracheally.**

867 Experiments were terminated on Day 61 post-infection. Data are from *n*=6-7 total mice

868 per group from *N*=2 independent experiments. *, $P < 0.05$. ***, $P < 0.001$.

869

870 **S2 Fig. Effects of monocyte ablation on derivative cells, pulmonary cytokines,**

871 **and lung pathology.**

872 (A-E) Flow cytometry of lung cells from naive and infected WT littermates and infected

873 CCR2-DTR^{+} mice, including Ly6C^{hi} monocytes (A), Ly6C^{lo} monocytes (B), alveolar

874 macrophages (C), interstitial macrophages (D), and moDCs (E). Data include *n*=6 total

875 naive mice from *N*=2 independent experiments; Day 3 is *n*=15-19 total mice per infected

876 group from *N*=3 independent experiments; and Day 7 is *n*=5 total mice per infected

877 group from *N*=1 experiments. (F-G) Pulmonary levels of GM-CSF (F), MCP-1/CCL2 (G),

878 IL-1α (H), and IL-1β (I). Results are from *n*=8-9 total mice per group per timepoint from

879 *N*=2 independent experiments. (J) Representative images of unaltered whole lungs

880 surgically collected from WT littermate and CCR2-DTR^{+} mice at Day 7 p.i. (K-N)

881 Representative Masson's trichrome stain of lung sections from WT littermate and

882 CCR2-DTR^{+} mice comparing alveoli (I-J), scale bar = 100μM at 10X magnification, and

883 bronchovascular bundles (K-L), scale bar = 25μM at 40X magnification. Airway (AW);

884 Blood vessel (BV); Collagen fibers (black arrows); Fungal cells (yellow arrowheads).

885 Data presented as mean ± SEM and analyzed using two-way ANOVA (A-I). *, P <0.05.
886 **, P <0.01. ***, P <0.001. ****, P <0.0001.
887
888 **S3 Fig. Dendritic cells do not have a role in the response to *C. gattii* infection.**
889 (A-B) Flow cytometry of dendritic cells from the lungs of MHCII$^{fl/fl}$ controls (black
890 line/white circles) and CCR2-Cre^{+} MHCII$^{fl/fl}$ mice (orange filled line/orange circles) at
891 Day 7 p.i., including a histogram of MHCII expression (A) and total numbers (B) of
892 CD11b^{+} conventional DC (cDC), CD103^{+} cDC, and monocyte-derived DCs (moDCs).
893 Data are n=6-10 total mice per group from N=2 independent experiments. (C) Kaplan-
894 Meier survival curve of MHCII$^{fl/fl}$ and CCR2-Cre^{+} MHCII$^{fl/fl}$ mice, n=8-10 total mice per
895 group from N=2 independent experiments. (D-F) Fungal burden was measured from
896 lung (D), MLN (E), and brain (F) at Day 7 p.i. Data are n=7-9 total mice per group from
897 N=2 independent experiments. (G-H) Flow cytometry of lung cells including CD11b^{+}
898 cDC (G) and CD103^{+} cDC (H) from WT and *Csf2*$^{-/-}$ mice at Days 5 and 10 p.i. Data are
899 n=5-8 total mice per group per time point from N=1-2 independent experiments. (I-J)
900 Flow cytometry of lung cells from naive and infected WT littermates and infected CCR2-
901 DTR^{+} mice at Days 3 and 7 p.i., including CD11b^{+} cDC (I) and CD103^{+} cDC (J). Results
902 are from n=6 naive WT littermate mice from N=2 independent experiments and n=5 total
903 infected mice per group per timepoint from N=1 experiment. Data presented as mean ±
904 SEM and analyzed using two-way ANOVA (G-J), Mann-Whitney test (B, D-F), or
905 Mantel-Cox test (C). ns, not significant. *, P <0.05. **, P <0.01. ***, P <0.001. ****, P
906 <0.0001.
907

908 **S4 Fig. Pulmonary Th1 and Th2 cytokines and chemokines in WT versus *Csf2*$^{-/-}$**
909 **mice.**
910 (A-C) Levels of pulmonary cytokines in infected WT and *Csf2*$^{-/-}$ mice including Th1-
911 associated and inflammatory cytokines (A), Th2-associated cytokines (B), and
912 chemokines (C). Results are from *n*=5-10 total mice per group per timepoint from *N*=1-2
913 independent experiments. Data presented as mean ± SEM and analyzed using two-way
914 ANOVA. *, $P < 0.05$. **, $P < 0.01$. ***, $P < 0.001$. ****, $P < 0.0001$.
915
916 **S5 Fig. Pulmonary Th1 and Th2 cytokines and chemokines in WT littermate**
917 **versus CCR2-DTR^{+} mice.**
918 (A-C) Levels of pulmonary cytokines in infected WT littermate and CCR2-DTR^{+} mice
919 including Th1-associated and inflammatory cytokines (A), Th2-associated cytokines (B),
920 and chemokines (C). Results are from *n*=5-10 total mice per group per timepoint from
921 *N*=1-2 independent experiments. Data presented as mean ± SEM and analyzed using
922 two-way ANOVA. *, $P < 0.05$. **, $P < 0.01$. ***, $P < 0.001$. ****, $P < 0.0001$.
923
924 **S6 Fig. GM-CSF and monocyte-derived macrophages promote airway**
925 **inflammation.**
926 (A-B) Representative Masson's trichrome stained sections showing large airways, small
927 airways, and terminal airways in the lungs of WT and *Csf2*$^{-/-}$ mice at Day 10 p.i. (A) and
928 WT littermate and CCR2-DTR^{+} mice at Day 7 p.i. (B). Images in the left panels for each
929 mouse strain are shown with scale bar = 100μM at 10X magnification. Black boxes
930 represent magnified insets shown in the right panels for each mouse strain, with scale

931 bar = 12μM at 60X magnification. Fungal cells (yellow arrowheads), goblet cells (green
932 arrowheads); subepithelial layer (orange arrows).
933
934 **S7 Fig. Gating strategy for macrophage, monocyte, and granulocyte cell**
935 **populations in murine lungs by flow cytometry.**
936 Lung cells from a naive CCR2-DTR^{+} mouse were collected for flow cytometry analysis.
937 Gating strategy for macrophages (CD45^{+}CD64^{+}MerTK^{+}) including alveolar
938 macrophages (CD11b^{-}CD11c^{hi}SiglecF^{+}) and interstitial macrophages
939 (CD11b^{+}CD11c^{+}SiglecF^{-}); monocytes (CD45^{+}CD64^{+}MerTK^{-}CD11c^{-}SiglecF^{-}CD11b^{+})
940 including Ly6C^{hi} monocytes and Ly6C^{lo} monocytes; and granulocytes
941 (CD45^{+}CD64^{-}MHCII^{--}CD11c^{-}CD11b^{+}SSC^{hi}) including neutrophils (Ly6G^{+}SiglecF^{-}) and
942 eosinophils (Ly6G^{-}SiglecF^{+}).
943
944 **S8 Fig. Gating strategy for dendritic cell subsets in murine lungs by flow**
945 **cytometry.**
946 Lung cells from a naïve CCR2-DTR^{+} mouse were collected for flow cytometry analysis.
947 This strategy first excludes SiglecF^{+}, MerTK^{+}, CD3^{+}, and CD19^{+} cells and then identifies
948 DCs (CD45^{+}CD3^{-}CD19^{-}MerTK^{-}SiglecF^{-} MHCII^{hi} CD11c^{+}) including CD11b^{+} cDCs
949 (CD64^{-}CD11b^{+}CD103^{-}), CD103^{+} cDCs (CD64^{-} CD11b^{-}CD103^{+}), and moDCs
950 (CD64^{+}CD11b^{+} CD103^{-}).
951
952

953 **S9 Fig. Gating strategy for MHCII expression by DCs in the lungs of CCR2-Cre^{+}**

954 **MHCII$^{fl/fl}$ mice.**

955 Lung cells from MHCII$^{fl/fl}$ littermate controls were collected for flow cytometry analysis on

956 Day 7 p.i. This strategy first excludes SiglecF^{+}, MerTK^{+}, CD3^{+}, and CD19^{+} cells and

957 then separates monocyte-derived and non-monocyte-derived cells by CD64 histogram.

958 FSC-A^{hi} cells were selected for CD11b^{+} vs CD103^{+} gating. CD11b^{+} and CD103^{+} cDCs

959 and moDCs were then determined by using a MHCII expression overlay to determine

960 MHCII^{+} cell populations in the littermate control mice. These overlays were then applied

961 to DC gates in CCR2-Cre^{+} MHCII$^{fl/fl}$ samples.

962

963 **S1 Table. Conjugated antibodies used for flow cytometry experiments.**

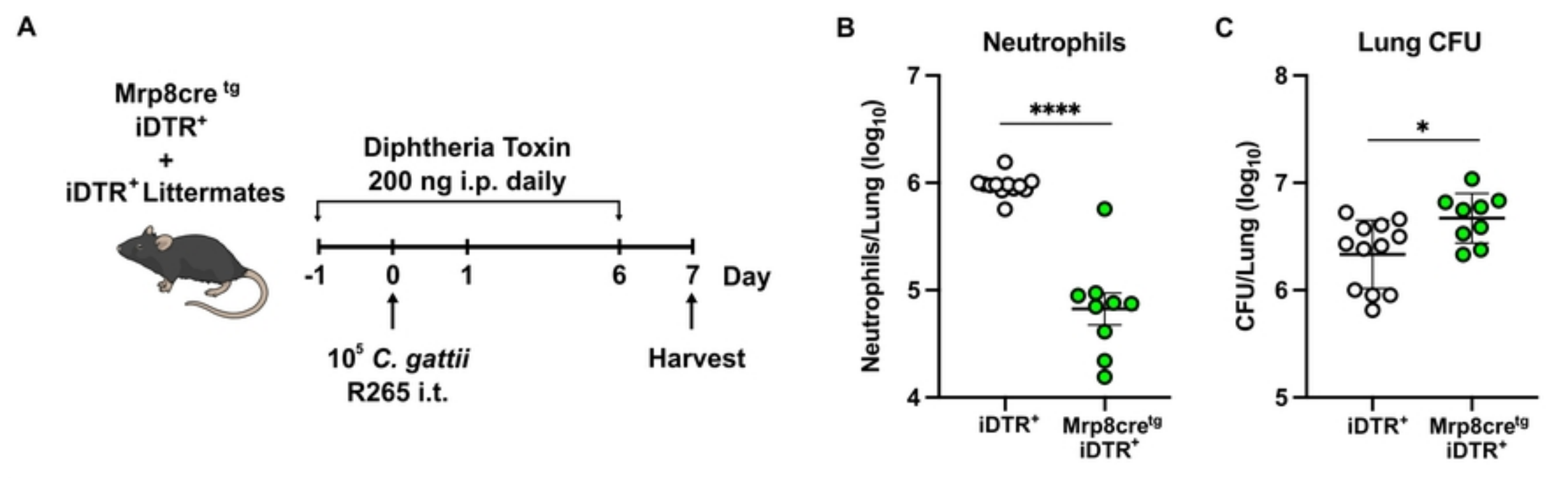
A
Mrp8cre tg
iDTR+
+
iDTR+ Littermates
Diphtheria Toxin
200 ng i.p. daily
-1
0
1
6
7
Day
10^5 C. gattii
R265 i.t.
Harvest
B
Neutrophils
Neutrophils/Lung (log10)
****
iDTR+
Mrp8cretg
iDTR+
C
Lung CFU
CFU/Lung (log10)
*
iDTR+
Mrp8cretg
iDTR+

Fig6

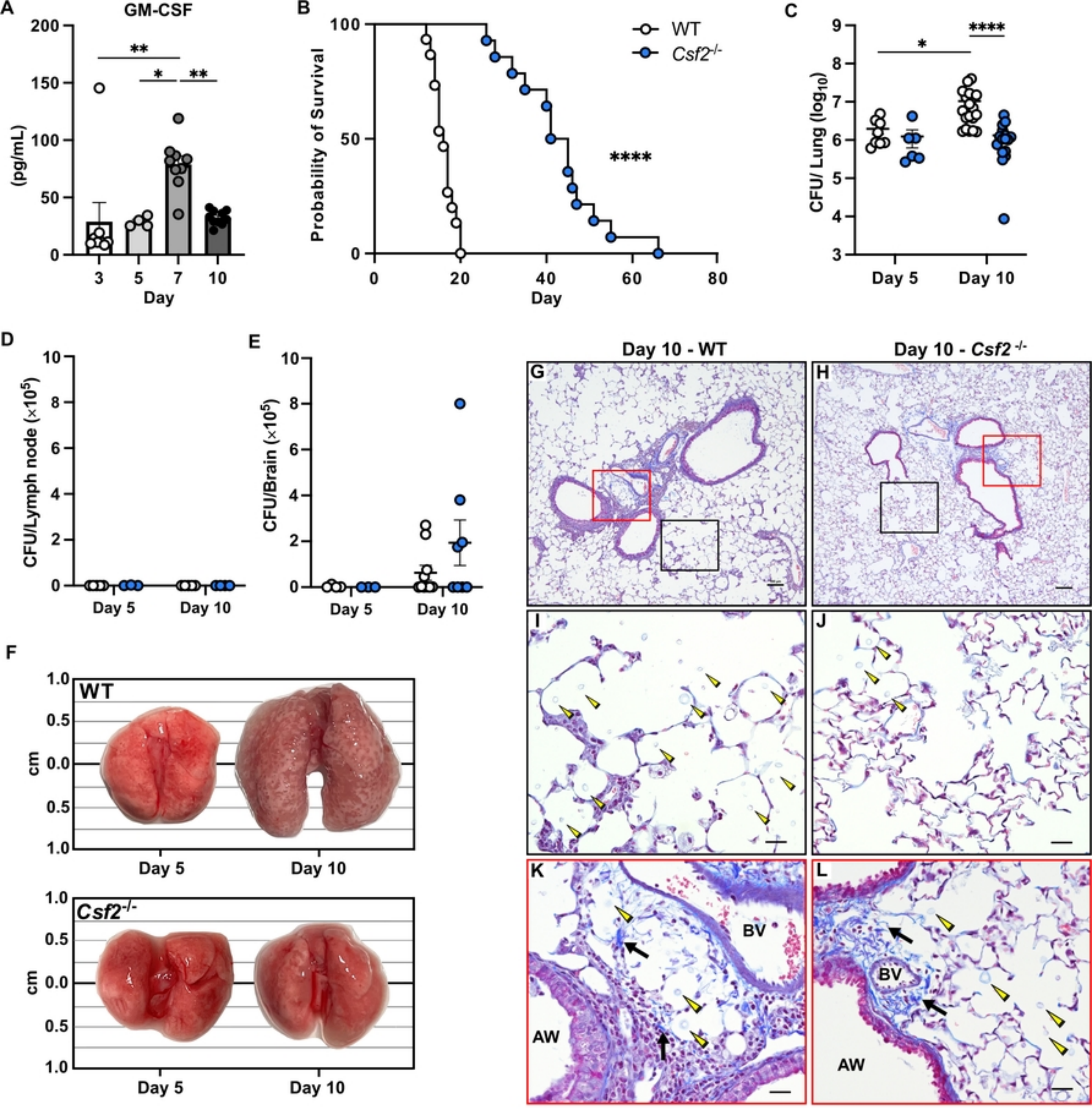
A
GM-CSF
(pg/mL)
Day
B
WT
Csf2-/-
Probability of Survival
Day
C
CFU/ Lung (log10)
Day 5
Day 10
D
CFU/Lymph node (×10^5)
Day 5
Day 10
E
CFU/Brain (×10^5)
Day 5
Day 10
F
WT
Csf2-/-
cm
Day 5
Day 10
Day 10 - WT
Day 10 - Csf2 -/-
G
H
I
J
K
L
BV
AW

Fig1

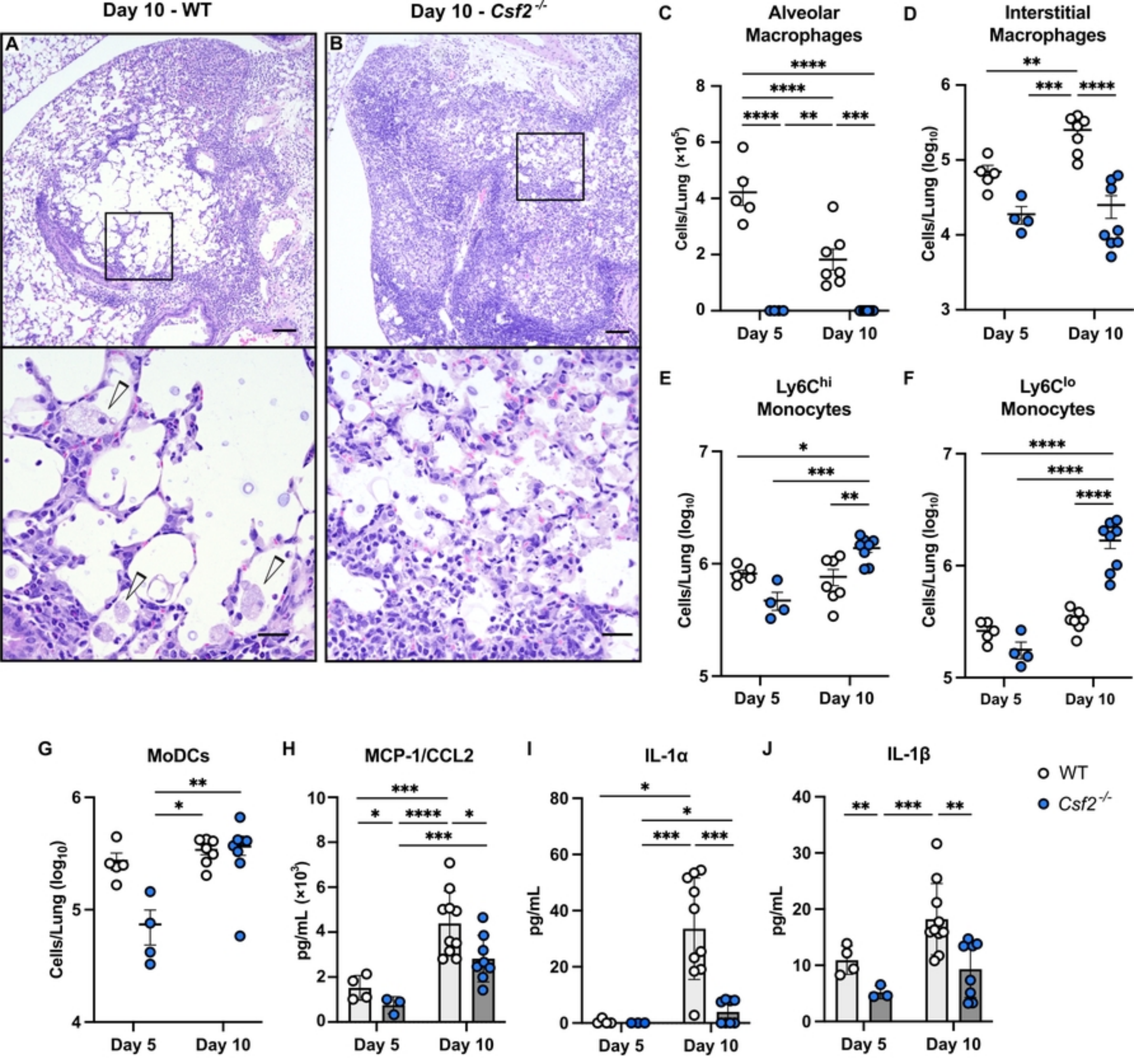
Day 10 - WT
Day 10 - Csf2-/-
A
B
C
Alveolar Macrophages
Cells/Lung (×10^5)
Day 5
Day 10
D
Interstitial Macrophages
Cells/Lung (log10)
E
Ly6Chi Monocytes
F
Ly6Clo Monocytes
G
MoDCs
H
MCP-1/CCL2
pg/mL (×10^3)
I
IL-1α
pg/mL
J
IL-1β
WT
Csf2-/-

Fig2

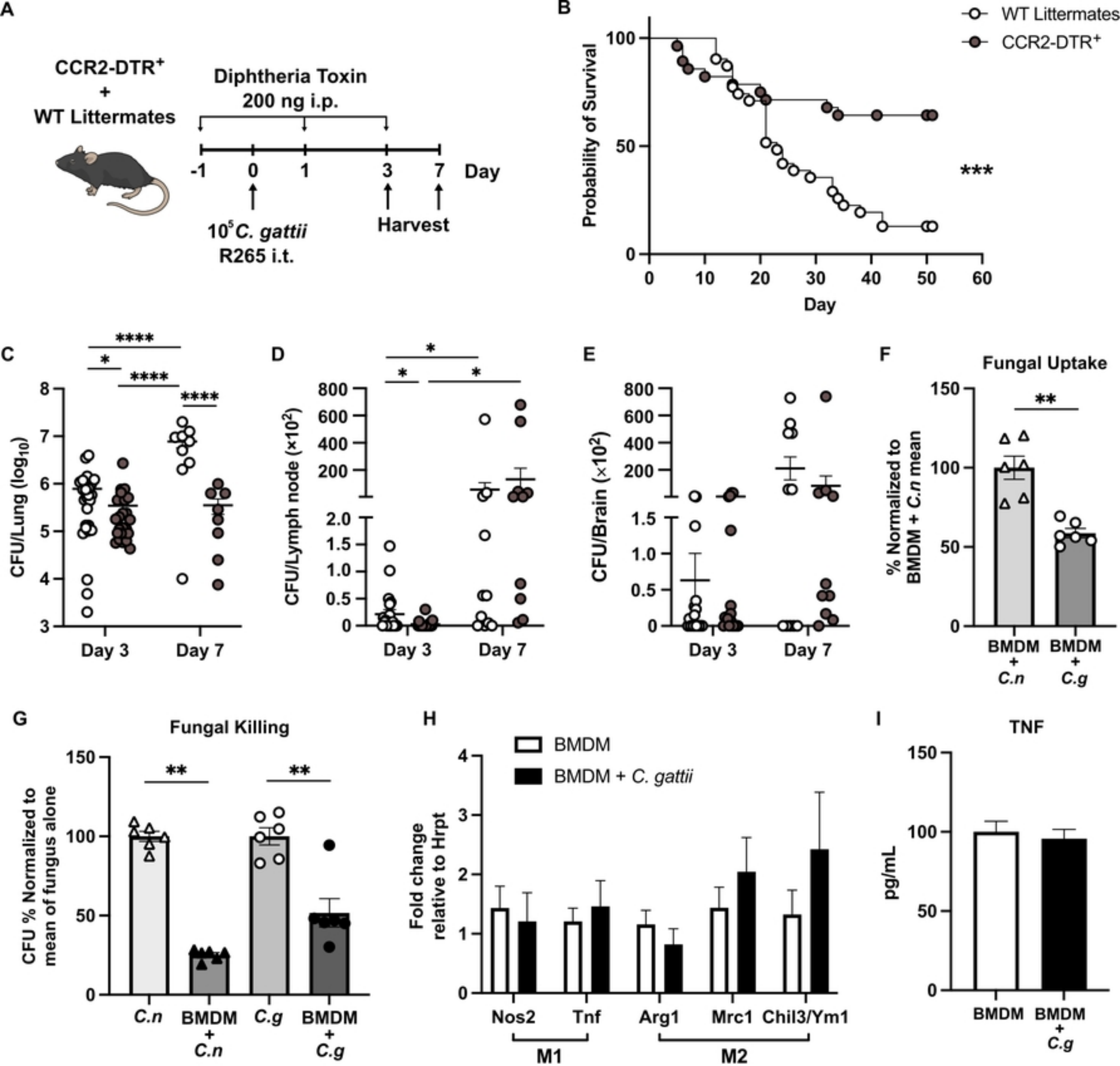
A
CCR2-DTR+
+
WT Littermates
Diphtheria Toxin
200 ng i.p.
-1
0
1
3
7
Day
10^5 C. gattii
R265 i.t.
Harvest
B
WT Littermates
CCR2-DTR+
Probability of Survival
Day
***
C
CFU/Lung (log10)
Day 3
Day 7
D
CFU/Lymph node (×10^2)
Day 3
Day 7
E
CFU/Brain (×10^2)
Day 3
Day 7
F
Fungal Uptake
% Normalized to BMDM + C.n mean
BMDM + C.n
BMDM + C.g
G
Fungal Killing
CFU % Normalized to mean of fungus alone
C.n
BMDM + C.n
C.g
BMDM + C.g
H
BMDM
BMDM + C. gattii
Fold change relative to Hrpt
Nos2
Tnf
Arg1
Mrc1
Chil3/Ym1
M1
M2
I
TNF
pg/mL
BMDM
BMDM + C.g

Fig3

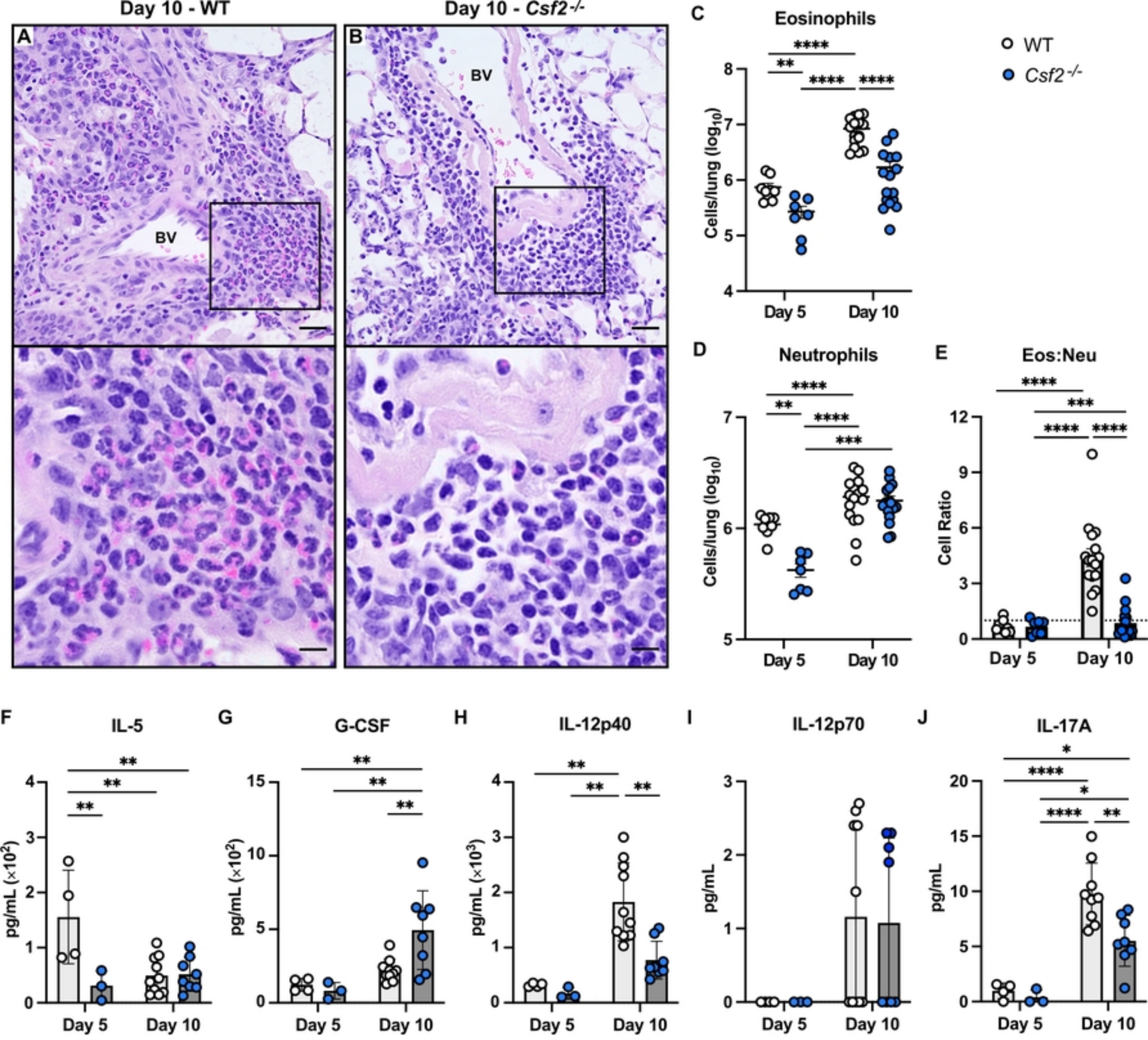
Day 10 - WT
Day 10 - Csf2-/-
A
B
BV
BV
C
Eosinophils
WT
Csf2-/-
Cells/lung (log10)
Day 5
Day 10
D
Neutrophils
Cells/lung (log10)
E
Eos:Neu
Cell Ratio
F
IL-5
pg/mL (×10^2)
G
G-CSF
pg/mL (×10^2)
H
IL-12p40
pg/mL (×10^3)
I
IL-12p70
pg/mL
J
IL-17A
pg/mL

Fig4

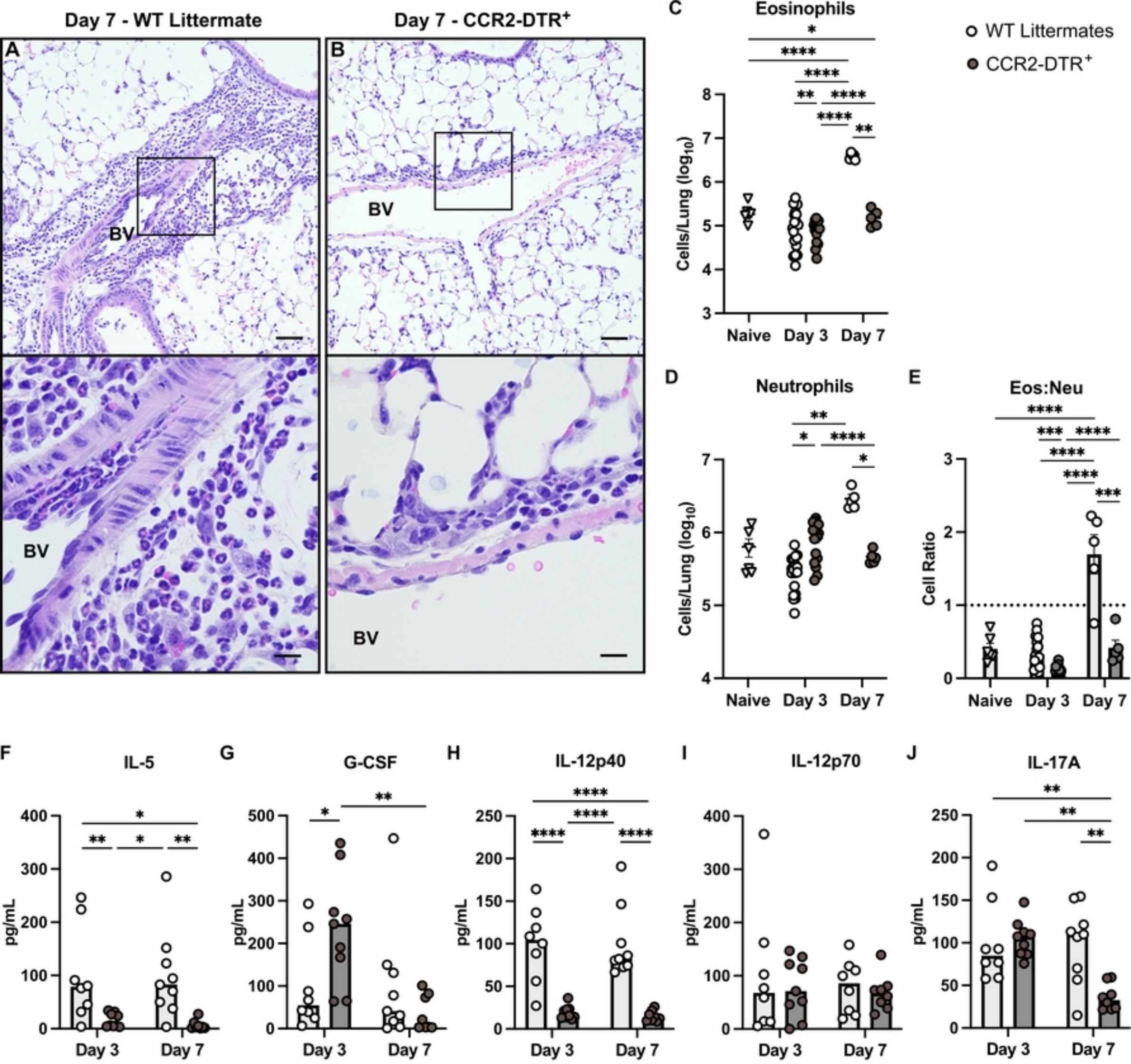
Day 7 - WT Littermate
Day 7 - CCR2-DTR+
A
B
BV
C
Eosinophils
WT Littermates
CCR2-DTR+
Cells/Lung (log10)
Naive
Day 3
Day 7
D
Neutrophils
E
Eos:Neu
Cell Ratio
F
IL-5
G
G-CSF
H
IL-12p40
I
IL-12p70
J
IL-17A
pg/mL

Fig5

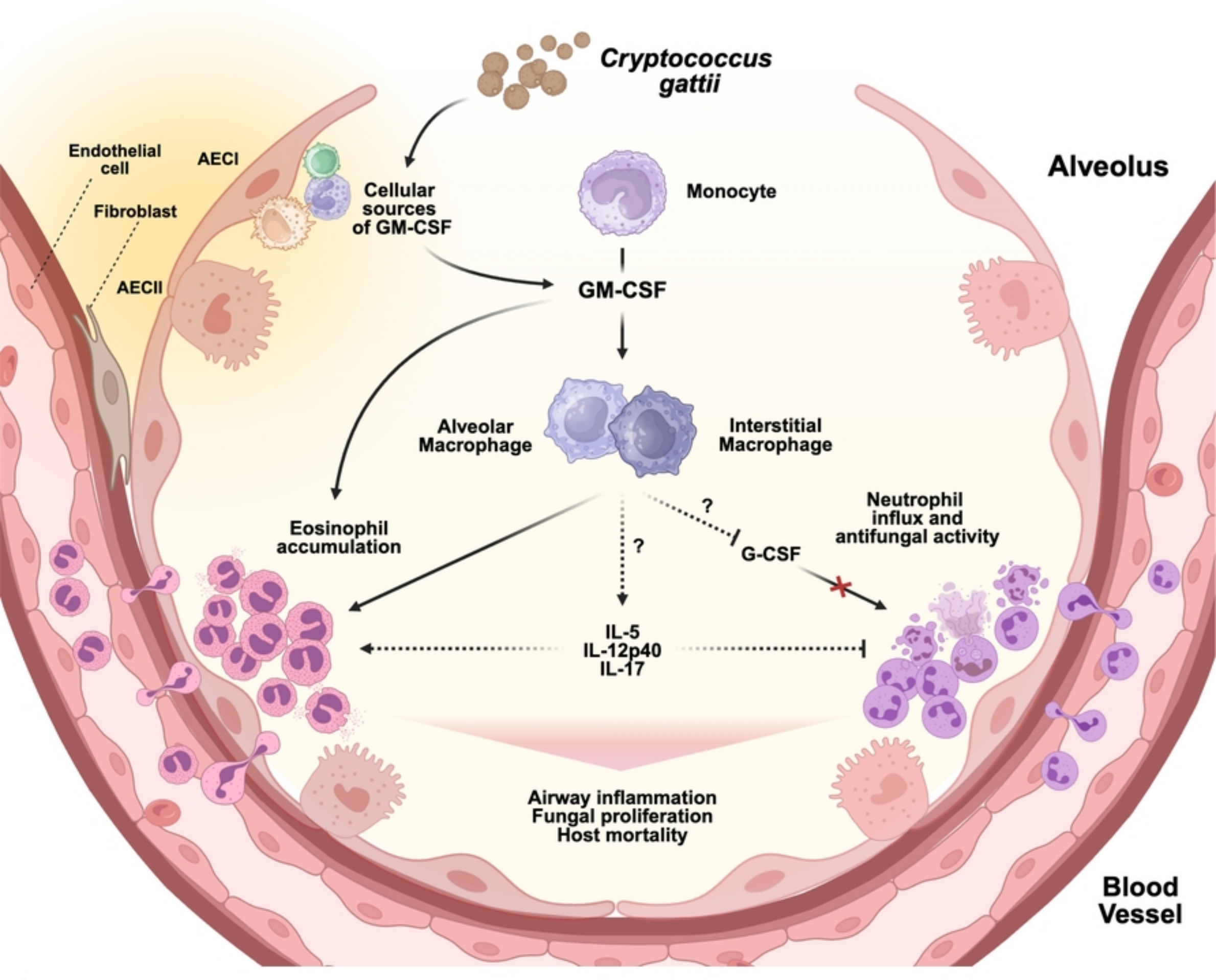
Cryptococcus gattii
Endothelial cell
AECI
Fibroblast
AECII
Cellular sources of GM-CSF
Monocyte
GM-CSF
Alveolus
Alveolar Macrophage
Interstitial Macrophage
Eosinophil accumulation
?
?
G-CSF
Neutrophil influx and antifungal activity
IL-5
IL-12p40
IL-17
Airway inflammation
Fungal proliferation
Host mortality
Blood Vessel

Fig7